TMEM165 replenishes lysosomal Ca^{2+} stores, protects cells against Ca^{2+} overload, and mediates Ca^{2+}-induced lysosomal H^+ leakage

Authors:

Ran Chen,[1*] Bin Liu,[1*†‡] Dawid Jaślan,[2*] Lucija Kucej,[1] Veronika Kudrina,[2] Belinda Warnke,[2] Yvonne Klingl,[2] Arnas Petrauskas, [2] Kenji Maeda,[1] Christian Grimm,[2,3†] Marja Jäättelä,[1,4†]

Affiliations:

[1]Cell Death and Metabolism, Center for Autophagy, Recycling and Disease (CARD), Danish Cancer Institute, Copenhagen, Denmark

[2]Walther Straub Institute of Pharmacology and Toxicology, Faculty of Medicine, Ludwig-Maximilians-Universität, Munich, Germany

[3]Immunology, Infection and Pandemic Research IIP, Fraunhofer Institute for Translational Medicine and Pharmacology ITMP, Munich/Frankfurt, Germany

[4]Department of Cellular and Molecular Medicine, Faculty of Health Sciences, University of Copenhagen, Copenhagen, Denmark

[*]Equal contribution

[†]Correspondence: ubnl@novonordisk.com (B.L.), christian.grimm@med.uni-muenchen.de (C.G.) and mj@cancer.dk (M.J.)

‡Present address: Rare Disease, Novo Nordisk, Måløv, Denmark

Abstract

The proper function of lysosomes depends on their ability to store and release calcium. While several lysosomal calcium release channels have been described, how mammalian lysosomes replenish their calcium stores has not been determined. Using genetic depletion and overexpression techniques combined with electrophysiology and visualization of subcellular ion concentrations and their fluxes across the lysosomal membrane, we show here that TMEM165 imports calcium to the lysosomal lumen and mediates calcium-induced lysosomal proton leakage. Accordingly, TMEM165 accelerates the recovery of cells from cytosolic calcium overload thereby enhancing cell survival while causing a significant acidification of the perilysosomal area and the entire cytosol. These data indicate that in addition to its essential role in the glycosylation in the Golgi, a small but significant fraction of TMEM165 localizes on the lysosomal limiting membrane, where it protects cells against cytosolic calcium overload, preserves lysosomal function by refilling lysosomal calcium stores and regulates perilysosomal and lysosomal pH.

Key words: calcium; electrophysiology; lysosome; pH; TMEM165; TMEM175

40 **Introduction**

41 Calcium (Ca^{2+}) and proton (H^+) homeostasis are of crucial importance for virtually all aspects of
42 cellular life. In mammalian cells, the free Ca^{2+} concentration in the cytosol $[Ca^{2+}]_{cyt}$ is maintained
43 approximately four orders of magnitude lower than that in the extracellular space and the major
44 intracellular Ca^{2+} storage organelles [1, 2]. Similarly, the concentration of protons in the cytosol $[H^+]_{cyt}$
45 is up to three orders of magnitude lower than that in the lumen of lysosomes [2]. Such steep ion
46 concentration gradients across cellular membranes are maintained by numerous pumps, and
47 exchangers that remove excess Ca^{2+} and H^+ from the cytosol to their storage organelles or the
48 extracellular space [1, 3, 4]. Due to the effective cytosolic buffering systems for both ions, cells tolerate
49 transient fluctuations in their concentrations. In fact, such fluctuations are essential for a wide
50 range of physiological signaling cascades [1, 5]. Greater and more sustained changes in ion
51 homeostasis are, however, associated with pathological processes, and prolonged increases in
52 either $[Ca^{2+}]_{cyt}$ or $[H^+]_{cyt}$ eventually lead to cell death and organ dysfunction [6, 7].

53 Late endosomes/lysosomes (hereafter referred to as lysosomes) are membrane-
54 surrounded intracellular organelles originally described as sites of degradation and recycling of
55 cellular organelles and macromolecules [8, 9]. In recent years, lysosomes have emerged as versatile
56 signaling organelles that regulate numerous cellular functions from metabolic pathways and cell
57 division to malignant transformation and cell death [10-13]. Most, if not all, lysosomal activities
58 depend on ion channels and transporters that establish electrolyte concentration gradients and
59 membrane potential across the lysosomal limiting membrane [2, 14]. Due to the low pH optimum of
60 most lysosomal hydrolases, the catabolic function of lysosomes depends on the vacuolar-type H^+-
61 ATPase (V-ATPase), which continuously pumps protons from the cytosol to the lysosomal lumen [15,
62 16]. On the other hand, TMEM175, a H^+-activated and H^+-permeable channel in the lysosomal
63 limiting membrane, protects lysosomes from overacidification by leaking H^+ in response to low
64 luminal pH [17, 18]. The significant alkalization of TMEM175-depleted lysosomes observed upon V-
65 ATPase inhibition suggests that TMEM175 is not the only protein capable of releasing H^+ from the
66 lysosomal lumen [17].

67 The endoplasmic reticulum (ER), Golgi, and lysosomes constitute major intracellular Ca^{2+}
68 stores that can release Ca^{2+} to the cytosol in response to various second messengers activated by
69 intra- and extracellular cues [1, 19, 20]. While the sarco/endoplasmic reticulum Ca^{2+} ATPases (SERCAs)
70 constantly pump free cytosolic Ca^{2+} to the ER, and SERCA and secretory pathway Ca^{2+} ATPases
71 pump it to the Golgi, the mechanisms by which mammalian lysosomes replenish their Ca^{2+} stores
72 remain largely unknown. In plant and yeast cells, the Ca^{2+} filling of their lysosome-related
73 organelles, vacuoles, is mediated by Ca^{2+}/H^+ exchangers CAX and VCX1, respectively [21, 22]. Although

74 strong experimental evidence suggests that a similar Ca^{2+}/H^{+} exchanger activity drives lysosomal
75 Ca^{2+} filling in mammalian cells, CAX and VCX1 have neither mammalian orthologs nor known
76 functional counterparts [20, 21]. Given that the V-ATPase constitutively pumps cytosolic H^{+} into the
77 lysosomal lumen, the resulting steep H^{+} gradient across the lysosomal membrane could in theory
78 provide the driving force for a putative lysosomal Ca^{2+}/H^{+} exchanger. Such an exchanger could also
79 explain the TMEM175-independent lysosomal H^{+} leakage discussed above and the cytosolic
80 acidification observed in response to elevated $[Ca^{2+}]_{cyt}$ observed for example in glutamate-treated
81 rat sensory neurons [23], ionomycin-treated rabbit corneal epithelial cells [24], rat parotid and
82 pancreatic acinar cells treated with various Ca^{2+} mobilizing agents [25, 26], and human cancer cells
83 treated with cationic amphiphilic drugs (CADs) that trigger lysosomal Ca^{2+} release via the purinergic
84 receptor P2X4 (P2RX4) and subsequent lysosome-dependent cancer cell death [27].
85 In living cells, the lysosomal H^{+} leakage has hitherto been demonstrated only indirectly by
86 measuring changes in the lysosomal and cytosolic pH. To detect the lysosomal H^{+} leakage directly,
87 we created a spatially restricted pH sensor that allowed us to measure local pH changes in the
88 perilysosomal area. Using this tool, we confirmed the TMEM175-mediated basal lysosomal H^{+}
89 leakage in living cells and demonstrated that TMEM175-independent perilysosomal acidification
90 occurs in response to various Ca^{2+} mobilizing agents. The latter triggered a search for a lysosomal
91 Ca^{2+}/H^{+} exchanger and the identification of TMEM165, which has been previously described as a
92 putative cation/H^{+} antiporter that exchanges Ca^{2+} and manganese (Mn^{2+}) for H^{+} across the Golgi
93 membrane [28], as a mediator of Ca^{2+}-induced lysosomal H^{+} leakage in mammalian cells. Taken
94 together, our data provide a molecular explanation for the long-sought Ca^{2+} influx pathway into
95 lysosomes.
96

97 **Results**

98 **Lysosomal proton leakage acidifies the perilysosomal area**

99 To visualize lysosomal H^{+} efflux in living cells, we constructed a cDNA encoding for a perilysosomal
100 pH sensor consisting of 39 amino-terminal amino acids of late endosomal/lysosomal adaptor, MAPK
101 and MTOR activator 1 (LAMTOR1), which target the protein to the lysosomal surface [29], and a pH-
102 sensitive fluorescent protein, mKeima, whose fluorescence intensity negatively correlates with the
103 adjacent pH [30] (Fig. 1a,b). In stably transfected HeLa human cervix carcinoma cells, the obtained
104 Lyso-mKeima sensor colocalized mainly with established lysosomal markers, Lysotracker® green
105 (LTG) and monomeric green fluorescence (mGFP)-tagged lysosomal associated membrane protein 1
106 (LAMP1) but not with the Golgi apparatus visualized by enhanced GFP (EGFP)-tagged RAB6A [31], ER
107 visualized by ER-tracker™ Green or mitochondria visualized by Mitotracker™ Green (Fig. 1a and

108 Extended Data Fig. 1a-c). Using Lyso-mKeima and either SypHer3s or pHrodo™-Green-AM to
109 detect perilysosomal and cytosolic pH, respectively, we demonstrated that the H^+ concentration on
110 the lysosomal surface of HeLa cells (pH 7,05 ± 0.01) was 2.9-fold higher than that in the cytosol (pH
111 7.52 ± 0.03) (Fig. 1c). Substantial acidification of the perilysosomal area was also observed in all the
112 other human cell lines tested, *i.e.* in MCF7 (2.2-fold), MDA-MB-231 (1.6-fold) and MDA-MB-468
113 (2.1-fold) breast carcinoma cells and in noncancerous MCF10A breast epithelial cells (1.6-fold) (Fig.
114 1c and Extended Data Fig. 1d). In further support of the lysosomal H^+ leakage as the cause of the
115 perilysosomal acidification, siRNA-mediated partial depletion of the lysosomal H^+-activated H^+
116 channel TMEM175 in HeLa-Lyso-mKeima cells significantly increased the perilysosomal pH (Fig.
117 1d,e). Further supporting the existence of TMEM175-mediated basal lysosomal H^+ leakage, Lyso-
118 mKeima fluorescence increased slightly but significantly upon concanamycin A-mediated inhibition
119 of the V-ATPase in control cells but not in TMEM175-depleted cells (Fig. 1f). Even stronger increases
120 in Lyso-mKeima fluorescence intensities were observed upon treatment of HeLa cells with
121 arachidonic acid (Fig. 1g), which has been shown to induce a TMEM175-dependent decrease in
122 cytosolic pH (pH_{cyt}) [17]. In contrast to the reported complete inhibition in TMEM175 knockout (KO)
123 cells [17], TMEM175 siRNAs only partially inhibited the lysosomal H^+ efflux induced by arachidonic
124 acid (Fig. 1h).
125 Taken together, these data introduce Lyso-mKeima as a useful tool to detect perilysosomal
126 pH and lysosomal H^+ leakage and demonstrate that TMEM175-mediated basal lysosomal H^+ leakage
127 maintains the pH of the perilysosomal area significantly below the value of the average cytosolic
128 pH.
129
130 **An increase in $[Ca^{2+}]_{cyt}$ triggers lysosomal H^+ leakage**
131 Commonly used cationic amphiphilic drugs (CADs) including antihistamines, antidepressants and
132 antipsychotics are emerging as potent anticancer drugs [12]. As basic and membrane permeable
133 molecules, they accumulate in the lysosomal lumen, where they inhibit lysosomal function and
134 induce lysosomal membrane permeabilization specifically in cancer cells [32, 33]. We have previously
135 shown that treating cancer cells with CADs induces cytosolic acidification hours before any signs of
136 lysosomal membrane damage or cell death occur [34]. Supporting lysosomal H^+ efflux as the
137 mechanism of CAD-induced cytosolic acidification, the CAD antihistamines, ebastine and
138 terfenadine, triggered rapid and significant increases in the Lyso-mKeima fluorescence intensity
139 (Fig. 2a,b). Importantly, these increases originated from the entire cell population and from the
140 presence of dozens of Lyso-mKeima positive puncta *per* cell rather than from a few dying cells or

141 individual damaged lysosomes (Fig. 2a). Notably, CAD-induced lysosomal H^+ flux was insensitive to
142 depletion of TMEM175 (Fig. 2c).
143 To determine the regulatory mechanism of CAD-induced, TMEM175-independent
144 lysosomal H^+ leakage, we first examined the role of CAD-induced rapid Ca^{2+} release in this process.
145 Interestingly, siRNA-mediated depletion of P2RX4, a Ca^{2+} channel responsible for the CAD-induced
146 lysosomal Ca^{2+} release [27], effectively blocked ebastine- and terfenadine-induced perilysosomal
147 acidification in HeLa-Lyso-mKeima cells (Fig. 2d and Extended Data Fig. 2a), while neither the
148 slightly acidic pH on the surface of lysosomes in control siRNA-treated cells (Extended Data Fig. 2b)
149 nor its further acidification by maximal inhibition of the V-ATPase depended on P2RX4 (Extended
150 Data Fig. 2c).
151 The reliance of CAD-induced lysosomal H^+ leakage on the P2RX4 Ca^{2+} channel inspired us to further
152 explore the link between lysosomal Ca^{2+} release and perilysosomal acidification. Given that the
153 elevation in the $[Ca^{2+}]_{cyt}$ controls diverse cellular functions and that lysosomal Ca^{2+} uptake has been
154 reported to depend on acidic lysosomal pH [21, 35], we investigated the possibility that lysosomes
155 export H^+ in exchange for importing excessive cytosolic Ca^{2+}. For this purpose, we treated the Lyso-
156 mKeima-expressing HeLa cells with three stimuli that increase the $[Ca^{2+}]_{cyt}$ via different means: (i)
157 thapsigargin, which inhibits the ER and Golgi resident SERCA Ca^{2+} pumps [36], (ii) ATP, which
158 stimulates P2 purinoreceptors to generate inositol 1,4,5-triphosphate (IP_3), which in turn triggers
159 the release of Ca^{2+} from the ER through IP_3 receptor-regulated channels [37], and (iii) ML-SA1, an
160 agonist of the lysosomal Ca^{2+} release channel, mucolipin TRP cation channel 1 (TRPML1) [38].
161 Following rapid and transient increases in the $[Ca^{2+}]_{cyt}$ (Fig. 2e, *top*), all three treatments induced
162 significant increases in Lyso-mKeima fluorescence intensity, which was indicative of decreased
163 perilysosomal pH and lysosomal H^+ leakage (Fig. 2e, *bottom*). In contrast to the transient $[Ca^{2+}]_{cyt}$
164 peak induced by thapsigargin, ATP, and ML-SA1, the Ca^{2+} peak induced by CADs was weaker and
165 longer lasting (Fig. 2e, *top*) [27], and was followed by a more substantial and persistent decrease in
166 perilysosomal pH (Fig. 2e, *bottom* and Extended Data Fig. 2d). Like CADs, thapsigargin and ML-SA1
167 induced TMEM175 independent lysosomal H^+ effluxes (Fig. 2f). However, the lysosomal H^+ efflux
168 triggered by thapsigargin was effectively inhibited by pretreatment of cells with the intracellular
169 Ca^{2+} chelator, BAPTA-AM (Fig. 2g).
170 The data presented above corroborate the ability of excess cytosolic Ca^{2+} to trigger
171 lysosomal H^+ leakage.
172
173 **TMEM165 mediates Ca^{2+}-induced lysosomal proton leakage**

174 In our search for a protein mediating Ca^{2+} influx into lysosomes, transmembrane protein 165
175 (TMEM165), a putative divalent cation/H^+ exchanger with a well-described role in manganese
176 homeostasis and glycosylation of proteins and lipids in the Golgi network [28, 39-41], attracted our
177 attention. In addition to its presence in the Golgi apparatus, TMEM165 has been detected in the
178 lysosomal compartment of HeLa cells, where its depletion has been reported to increase the
179 volume of the acidic compartment [28, 42]. Supporting the role of TMEM165 in CAD-induced,
180 lysosomal H^+ leakage, partial depletion of this gene by two independent siRNAs effectively reduced
181 ebastine- and terfenadine-induced lysosomal H^+ leakage and subsequent acidification of the cytosol
182 in HeLa cells (Fig. 3a-c). The strong TMEM165 dependences of CAD-induced lysosomal H^+ leakage
183 and cytosolic acidification were also observed in MDA-MB-468 and MCF7 cells, respectively
184 (Extended Data Fig. 3a-f). The depletion of *TMEM165* in HeLa and MDA-MB-468 cells also inhibited
185 lysosomal H^+ leakage induced by other Ca^{2+}-mobilizing agents, ML-SA1 and thapsigargin (Fig. 3d and
186 Extended Data Fig. 3g), while TMEM165 was dispensable for the perilysosomal acidification induced
187 by arachidonic acid and concanamycin A (Extended Data Fig. 3h,i). Furthermore, siRNA-mediated
188 depletion of TMEM165 had no effect on the perilysosomal pH in untreated HeLa cells (Fig. 3e), and
189 even complete CRISPR-mediated depletion of TMEM165 in either HeLa or MDA-MB-468 cells
190 altered neither the lysosomal nor the cytosolic pH in unstimulated cells (Fig. 3f-h and Extended
191 Data Fig. 3e,f,j). However, the overexpression of either TMEM165-Flag or TMEM165-mCherry in
192 HeLa cells significantly altered the intracellular pH homeostasis by increasing the lysosomal pH and
193 acidifying not only the perilysosomal area but also the entire cytosol (Fig. 3e-i).
194 These data indicate that TMEM165 is required for the lysosomal H^+ leakage in response to
195 elevations in the free $[Ca^{2+}]_{cyt}$, and that its overexpression disturbs cellular pH homeostasis.
196
197 **TMEM165 replenishes lysosomal Ca^{2+} stores and protects cells against Ca^{2+} mobilizing agents**
198 Next, we investigated the effect of TMEM165 on the cellular Ca^{2+} homeostasis. To determine the
199 effect of TMEM165 on the capacity of lysosomes to store Ca^{2+}, we measured the fluorescence
200 intensity (FLI) of a cytosolic Ca^{2+} indicator Fluo4-AM following the mobilization of lysosomal Ca^{2+}
201 with glycyl-L-phenylalanine-beta-naphthylamide (GPN), a lysosomotrope that permeabilizes
202 lysosomal membranes in a cathepsin C-dependent manner [43, 44]. The increase in the free $[Ca^{2+}]_{cyt}$
203 upon lysosomal membrane permeabilization was significantly reduced or increased in TMEM165-
204 depleted and TMEM165-Flag expressing HeLa cells, respectively (Fig. 4a,b). Similarly, GPN-mediated
205 lysosomal membrane permeabilization significantly increased the free $[Ca^{2+}]_{cyt}$ less in MDA-MB-468-
206 TMEM165-KO cells than in parental MDA-MB-486 cells (Fig. 4c). In further support of the ability of
207 TMEM165 to fill lysosomal Ca^{2+} stores, the transient expression of TMEM165-mCherry in HEK293

208 human kidney epithelial cells increased the release of lysosomal Ca^{2+} upon ML-SA1-mediated
209 activation of the lysosomal TRPML1 Ca^{2+} channel, as determined by the fluorescence intensity of
210 the coexpressed TRPML1-GCaMP6s Ca^{2+} sensor (Extended Data Fig. 4a,b). Notably, the TMEM165-
211 R126C mutant, which has been reported to increase the lysosomal localization of TMEM165
212 without affecting its activity (ref [42]), increased the capacity of lysosomes to release Ca^{2+} in response
213 to ML-SA1 even more than the wild-type TMEM165 (Extended Data Fig. 4a,b). Both the wild-type
214 and the mutant TMEM165-mCherry colocalized with the lysosomal markers, LysoTracker and
215 LAMP1, and their localization on the lysosomal limiting membrane was visualized in lysosomes
216 enlarged by the PIKfyve inhibitor apilimod. (Extended Data Fig. 4c,d). Importantly, the transient
217 expression of neither TMEM165 construct altered the expression levels of the TRPML1-GCaMP6s
218 Ca^{2+} sensor (Extended Data Fig. 4e).
219 To study the perilysosomal free [Ca^{2+}] without disturbing cellular Ca^{2+} homeostasis, we
220 constructed a novel Ca^{2+} sensor, Lyso-GCaMP8s, by fusing the lysosomal membrane-targeting
221 amino terminus of LAMTOR1 to the amino terminus of the GCaMP8s Ca^{2+} sensor. Supporting the
222 role of TMEM165 in lysosomal Ca^{2+} influx, siRNA-mediated depletion of TMEM165 increased and
223 TMEM165-mCherry expression reduced the perilysosomal free [Ca^{2+}] in HeLa cells (Fig. 4d), and the
224 reintroduction of TMEM165 into MDA-MB-468-TMEM165-KO cells completely reverted the high
225 perilysosomal free [Ca^{2+}] phenotype of the TMEM165-KO cells (Fig. 4e). Notably, TMEM165
226 depletion did not alter the free [Ca^{2+}]$_{cyt}$ in unstimulated MDA-MB-468 cells indicating that
227 TMEM165 controls cellular Ca^{2+} homeostasis locally at the lysosomal membrane (Fig. 4f).
228 Accordingly, TMEM165 deficiency delayed the clearance of cytosolic Ca^{2+} in MDA-MB-468 cells
229 following ML-SA1-mediated activation of lysosomal TRPML1 Ca^{2+} channels but did not significantly
230 affect the removal of cytosolic Ca^{2+} after ATP-induced activation of IP_3 receptor-regulated Ca^{2+}
231 channels in the ER (Fig. 4f,g). However, MDA-MB-468-TMEM165-KO cells failed to recover from the
232 thapsigargin-induced cytosolic Ca^{2+} overload thereby revealing the potential of TMEM165 to clear
233 cytosolic Ca^{2+} in the absence of the activity of ER Ca^{2+} pumps (Fig. 4h). Notably, the prolonged
234 thapsigargin-induced cytosolic Ca^{2+} overload in TMEM165-deficient cells was associated with
235 significantly increased cell death (Fig. 4i). Prompted by these results, we investigated the effect of
236 TMEM165 on CAD-induced cancer cell death, which depends on lysosomal Ca^{2+} release and
237 activation of Ca^{2+}-dependent cyclic AMP synthesis [27]. Compared to the parental MDA-MB-468 cells,
238 TMEM165 deficiency significantly increased the ebastine-induced cytosolic Ca^{2+} overload, resulting
239 in almost 3-fold higher free [Ca^{2+}]$_{cyt}$ 1 h after the treatment, and increased the subsequent cell
240 death to a similar extent (Fig. 4j,k). TMEM165 deficient MDA-MB-468 cells displayed a similar
241 sensitization to terfenadine (Extended Data Fig. 4f). The crucial role of TMEM165 in protecting

242 cancer cells from CADs was confirmed in HeLa cells, where TMEM165 deficiency also increased the
243 CAD-induced cytosolic Ca^{2+} overload and cell death while the expression of TMEM165-mCherry
244 effectively inhibited both events (Fig. 4l-n). Notably, TMEM165-mCherry-mediated protection
245 against CAD-induced HeLa cell death was associated with a nearly complete inhibition of CAD-
246 induced formation of galectin 1 (LGALS1) puncta, indicative of the inhibition of lysosomal
247 membrane permeabilization (Fig. 4n) [45].
248 Taken together, these data reveal taht TMEM165 is essential for maintaining lysosomal
249 Ca^{2+} stores and protecting against cytosolic Ca^{2+} overload and subsequent lysosomal membrane
250 permeabilization.
251
252 **A fraction of TMEM165 localizes to the lysosomal limiting membrane**
253 TMEM165 was originally characterized as a Golgi resident protein, whose mutations cause
254 congenital disorders of glycosylation [39]. In line with the presence of the tyrosine-based, putative
255 lysosomal targeting signal ^{124}YNRL^{127} in the human TMEM165 protein, visualization of GFP- or RFP-
256 tagged TMEM165 has revealed that TMEM165 traffics to lysosomes via the plasma membrane [42].
257 To ensure that the TMEM165-mCherry used in this study also localized to lysosomal membranes,
258 we analyzed its localization in HeLa and MDA-MBA-468 cells. In HeLa cells, the overexpressed
259 TMEM165-mCherry formed strongly fluorescent punctuate structures colocalizing with the
260 lysosomal markers Lyso-GFP (r = 0.93 ± 0.05) and Lysotracker™ Green (r = 0.83 ± 0.05) and larger,
261 perinuclear sheet-like structures with weaker fluorescence intensity and colocalization with the
262 *trans*-Golgi marker EGFP-RAB6 (r = 0.42 ± 0.08) (Fig. 5a and Extended Data Fig. 5a). Indicating that
263 the observed lysosomal localization was not caused by the overexpression, TMEM165-mCherry,
264 which was expressed in MDA-MB-468-TMEM165-KO cells at a level similar to that of the
265 endogenous TMEM165 protein, exhibited a similar distribution pattern with high intensity
266 punctuate structures colocalizing with Lysotracker™ Green (r = 0.85 ± 0.02) and sheet-like weaker
267 intensity structures colocalizing with EGFP-RAB6 (r = 0.57 ± 0.12) (Extended Data Fig. 3e and 5b).
268 Importantly, the formation of larger lysosomes upon inhibition of PIKfyve by vacuolin-1 revealed
269 that also the stably expressed TMEM165-mCherry decorated lysosomal limiting membranes (Fig.
270 5a, *bottom*) [46], strongly suggesting that TMEM165-mCherry is a lysosomal membrane protein rather
271 than a lysosomal cargo. This was further supported by the similar lysosomal localization of
272 TMEM165-mCherry in cells in which autophagy was either pharmacologically (3-methyladenine) or
273 genetically (ATG7-KO) inhibited (Fig. 5b).
274 In line with previous reports [39, 42], immunostaining failed to reveal a significant
275 colocalization of either endogenous or overexpressed TMEM165 with lysosomal markers (Extended

276 Data Fig. 5c,d). To address this discrepancy, we realized that the localization of TMEM165-mCherry
277 in HeLa cells dramatically altered from punctuate and mainly lysosomal structures in live or fixed
278 cells to sheet-like and mainly Golgi-localized (colocalization with N-
279 acetylgalactosaminyltransferase-EGFP (Golgi-EGFP, *trans*-Golgi)) structures following the
280 permeabilization of fixed cells (Fig. 5a and Extended Data Fig. 5a,b,e). Due to this phenomenon, we
281 were not able to demonstrate the lysosomal localization of the endogenous TMEM165 by
282 immunostaining. Instead, we purified iron-dextran (FeDex)-loaded lysosomes from HeLa cells by
283 magnetic capture and analyzed the proteins in the obtained eluates by immunoblotting. A small
284 fraction of the endogenous TMEM165 was detected in the purified LAMP2-rich lysosomes, which
285 did not contain detectable proteins from endosomes (early endosome antigen 1 (EEA1) and cation-
286 independent mannose 6 phosphate receptor (CI-M6PR)), the Golgi (receptor-binding cancer
287 antigen expressed on SiSo cells (RCAS1), Golgi reassembly stacking protein 1 (GORASP1), and CI-
288 M6PR), the ER (protein disulfide isomerase (PDI)) or the plasma membrane (Na^+/K^+-ATPase) (Fig.
289 5c). However, the purified lysosomal fraction contained a small amount of mitochondrial import
290 receptor subunit TOM20 homolog (TOM20) possibly due to copurified mitochondria attached to
291 lysosomes or mitophagy (Fig. 6c). Notably, the inhibition of the V-ATPase by concanamycin A during
292 the lysosome purification procedure, which inhibits the degradation of cargo proteins in the
293 lysosomal lumen, did not significantly alter the level of TMEM165 in purified lysosomes, while the
294 putative cargo proteins Na^+/K^+-ATPase and CI-M6PR became detectable after concanamycin A
295 treatment (Fig. 5c).
296 Because the TMEM165-mediated maintenance of the Golgi Mn^{2+} homeostasis is essential
297 for the proper N-glycosylation of several membrane proteins [40], we next asked whether the
298 lysosomal phenotype observed in TMEM165 depleted cells could be a result of the defective
299 glycosylation of the normally highly lysosomal membrane proteins. Treatment with 1 μM $MnCl_2$ for
300 48 h completely reversed the hypoglycosylation phenotype in MDA-MB-468-TMEM165-KO cells as
301 demonstrated by the $MnCl_2$-induced reversal of the increased mobility of LAMP2 in sodium dodecyl
302 sulfate–polyacrylamide gel electrophoresis (Fig. 5d). However, the $MnCl_2$ supplementation rescued
303 neither the prolonged cytosolic Ca^{2+} peak nor the defective cytosolic acidification in CAD treated
304 MDA-MB-468-TMEM165-KO cells (Fig. 5e,f).
305 These data support the idea that a small fraction of TMEM165 localizes to the lysosomal
306 limiting membrane where it regulates lysosomal ion homeostasis.
307
308 **TMEM165 mediates H^+ and Ca^{2+} dependent currents**

309 The data presented above strongly suggest that TMEM165 plays a role in Ca^{2+} influx to the lysosome,
310 and H^+ efflux from the lysosome to the cytosol. To test this hypothesis, we performed patch-clamp
311 experiments using HEK293 cells transfected with wild-type TMEM165-mCherry, the R126C mutant,
312 or the mCherry vector as a control. We applied a step protocol from -100 mV to +60 mV with 20 mV
313 increments in the whole-cell mode with an asymmetrical pH (pipette 7.5/bath 4.6) and [Ca^{2+}] (pipette
314 1 µM/bath 10 nM) across the membrane mimicking the conditions in the cytosol (pipette) and the
315 lysosomal lumen (bath) (Fig. 6a). In cells expressing wild-type TMEM165-mCherry, we detected
316 significant inward current activity (most likely the net current of H^+ inward and Ca^{2+} outward) in a
317 physiologically relevant voltage range that was absent in control cells (Fig. 6b,c). TMEM165-R126C
318 mutant currents were considerably weaker than wild-type currents (Fig. 6b,c), while in the lysosomal
319 Ca^{2+} imaging experiments, the mutant protein had stronger effect on Ca^{2+} release than the wild-type
320 protein (Extended Data Fig. 4a,b). This difference is presumably due to the increased lysosomal and
321 decreased plasma membrane localization of the mutant protein (Fig. 6d; Extended Data Fig. 4c,d) (ref
322 [42]). Thus, we focused on wild-type TMEM165-mCherry and increased the bath pH from 4.6 to 7.5 with
323 the result that the measured inward current was almost completely reduced to zero (Fig. 6e,f, left).
324 Additionally, we reduced the Ca^{2+} concentration in the pipette from 1 µM to 10 nM, resulting in a
325 similar, almost complete loss of the current (Fig. 6e,f, middle). However, when omitting only Ca^{2+} we
326 noticed a comparably small reduction in the current (Fig. 6e,f, right), letting us to speculate that this
327 may be the result of the presence of 1 mM Mg^{2+}. We therefore next omitted both Ca^{2+} and Mg^{2+} from
328 the bath, now resulting in a complete loss of the current (Fig. 6g, left). When only Mg^{2+} was omitted,
329 the current decreased less (Fig. 6g, right) and remained significant in the TMEM165-expressing cells
330 when compared to control cells (Fig. 6h). These data suggest that the omission of either Ca^{2+} (in the
331 absence of Mg^{2+}) or H^+ significantly affects the observed current.
332 Although PIKfyve inhibitors enlarged TMEM-165-mCherry-positive lysosomes to some degree (Fig.
333 5g; Extended Data Fig. 4d), our efforts to detect TMEM165 currents across the lysosomal limiting
334 membrane were unfortunately hindered by the failure of PIKfyve inhibitors to trigger the formation
335 of large enough TMEM165-positive giant lysosomes for patch clamp, possibly due to TMEM165-
336 induced disturbances in the lysosomal Ca^{2+} homeostasis.
337 These data indicate that TMEM165 expression results in the voltage-dependent
338 development of H^+ and Ca^{2+} dependent currents, which are not present in controls. Thus, TMEM165

339 is indeed capable of transporting Ca^{2+} and Mg^{2+} ions into lysosomes and H^+ ions out of lysosomes in
340 an antiporter like manner.
341
342 **Discussion**
343 Lysosomal fitness depends on tightly regulated pH and Ca^{2+} concentration gradients across the
344 limiting membrane [2, 14]. While a low pH is essential for the activity of most lysosomal hydrolases,
345 the ligand-activated Ca^{2+} release through TRPML1, two pore channels, and P2RX4 governs
346 endolysosomal membrane trafficking and initiates numerous signaling cascades controlling for
347 example lysosomal biogenesis, cellular metabolism and lysosomal membrane stability [27, 47-49].
348 Despite the crucial role of lysosomal Ca^{2+} stores in the maintenance of lysosomal and cellular
349 health, the identity of the protein(s) responsible for filling mammalian lysosomes with Ca^{2+} remains
350 unknown. The data presented above identifies TMEM165 not only as a protein responsible for
351 maintaining lysosomal Ca^{2+} stores but also as a mediator of Ca^{2+}-induced lysosomal H^+ leakage in
352 mammalian cells. The role of TMEM165 in maintaining lysosomal Ca^{2+} stores is supported by ample
353 data showing i) a significant reduction in the amount of Ca^{2+} released to the cytosol upon GPN-
354 mediated lysosomal membrane permeabilization in TMEM165-depleted HeLa and MDA-MB-468
355 cells; ii) increased capacity of lysosomes to release Ca^{2+} in TMEM165 overexpressing HeLa and
356 HEK293-TRPLM1 cells upon treatment with GPN and ML-SA1, respectively; iii) TMEM165-
357 dependent recovery from the cytosolic Ca^{2+} overload in thapsigargin-, ML-SA1- and ebastine-
358 treated MDA-MB-468 cells and ebastine-treated HeLa cells; and finally, iv) the development of
359 voltage-dependent Ca^{2+} currents observed when patch-clamping TMEM165 overexpressing HEK293
360 cells. Previous studies have demonstrated the dependence of lysosomal Ca^{2+} influx on ER Ca^{2+}
361 stores, ER-lysosome contact sites and acidic lysosomal pH [9, 50-52]. The reported delay in the
362 inhibition of lysosomal Ca^{2+} influx following the disruption of the lysosomal pH gradient has,
363 however, suggested that the pH dependence of lysosomal Ca^{2+} influx observed in living cells is
364 caused by the disruption of ER-lysosome contact sites rather than the loss of the lysosomal pH
365 gradient [53]. In line with this, the removal of the pH gradient in our patch-clamp experiments had no
366 effect on TMEM165-mediated Ca^{2+} outward currents.
367 In addition to demonstrating the ability of TMEM165 to import Ca^{2+} from the cytosol to the
368 lysosome, our data also highlight the ability of TMEM165 to protect mammalian cells against Ca^{2+}
369 overload. This finding is in line with the reported sensitivity of the yeast strain depleted of the
370 TMEM165 ortholog Gdt1p (*gdt1*Δ) to high external Ca^{2+} concentrations, and the ability of the
371 amino-terminally truncated human TMEM165 to partially restore the growth of the *gdt1*Δ strain
372 under Ca^{2+} stress [28]. While the mammalian TMEM165 may play only a moderate role in the

373 clearance of cytosolic Ca^{2+} in general, its role in removing Ca^{2+} locally from the perilysosomal area is
374 likely to be of greater importance. This is clearly demonstrated by the substantial sensitization to
375 and inhibition of CAD-induced lysosome-dependent cancer cell death upon TMEM165 depletion
376 and overexpression, respectively. These data emphasize the role of P2RX4-mediated lysosomal Ca^{2+}
377 release in CAD-induced cancer cell death and are in line with our previous identification of Ca^{2+}-
378 dependent adenylate cyclase 1 as a mediator of CAD-induced lysosomal membrane
379 permeabilization and cell death [27, 34]. Providing further support for a link between the lysosomal
380 P2RX4 Ca^{2+} channel and TMEM165-mediated lysosomal H^+ leakage, a recent report describes a
381 significant, P2RX4-dependent increase in the lysosomal pH in metastatic breast cancer cells [54], and
382 the expression of both P2RX4 and TMEM165 has been linked to the metastatic potential of breast
383 cancer cells [54, 55].

384 To study the molecular basis of the lysosomal H^+ leakage conductance, we created a
385 fluorescent pH sensor, Lyso-mKeima, that detects the local pH on the surface of lysosomes. In the
386 meanwhile, Haoxing Xu and colleagues identified TMEM175 as the long-sought channel responsible
387 for the H^+-activated lysosomal H^+ leakage, which maintains a lysosomal pH of approximately 4.5 [17].
388 Using cytosolic pH indicators and Lyso-mKeima to measure cytosolic and perilysosomal pH,
389 respectively, we demonstrated a substantial TMEM175-dependent acidification of the
390 perilysosomal area in unstimulated HeLa cells and a further, TMEM175-independent acidification in
391 response to Ca^{2+}-mobilizing agents. The latter was effectively inhibited by the chelation of cytosolic
392 free Ca^{2+} by BAPTA-AM and by depletion of TMEM165, strongly suggesting that the TMEM165-
393 mediated lysosomal Ca^{2+} uptake triggers a TMEM165-dependent lysosomal H^+ leakage. This
394 hypothesis is strongly supported by our electrophysiological experiments demonstrating the ability
395 of TMEM165 to mediate voltage-dependent H^+ and Ca^{2+} dependent currents. The observed low pH
396 on the lysosomal surface in unstimulated cells, and especially its further, the TMEM165-dependent
397 long-lasting acidification induced by Ca^{2+} mobilizing agents is highly intriguing and argues against
398 the idea that variations in the cytosolic pH are insignificant, because cellular buffers quickly stabilize
399 them. Such drops in pH are known to alter the protonation status and function of several proteins,
400 for example phosphofructokinase, whose glycolytic activity regulates AMP-dependent protein
401 kinase (AMPK) on the lysosomal membrane [56, 57], and the GTP-binding protein RHEB, which controls
402 the activity of mammalian target of rapamycin complex 1 (mTORC1) by recruiting it to the
403 lysosomal membrane [58]. Thus, it is tempting to speculate that Ca^{2+}-induced acidification of the
404 perilysosomal area could contribute to the Ca^{2+} overload-induced shift from anabolic to catabolic
405 metabolism by altering the activity of AMPK, mTORC1 or other metabolic regulators residing on the
406 lysosomal membrane [12, 57, 59].

407 As discussed above, the maintenance of lysosomal H^+ and Ca^{2+} homeostasis is essential for
408 cellular fitness. Accordingly, their disturbances are associated with a wide range of pathologies
409 ranging from degenerative disorders to cancer [3, 4, 12, 16, 20, 60]. Thus, the identification of TMEM165 as
410 a regulator of lysosomal H^+ efflux and Ca^{2+} influx opens new avenues for the development of
411 therapeutics for the treatment of these diseases. In particular, TMEM165 antagonists and their
412 combination with CADs or other Ca^{2+} mobilizing cancer drugs could prove highly effective in the
413 future cancer treatment by increasing and prolonging the cytosolic Ca^{2+} overload and promoting
414 the subsequent lysosomal membrane permeabilization, while TMEM165 agonists could reverse
415 defective lysosomal Ca^{2+} stores in lysosomal storage disorders and assist the recovery of neurons
416 from the cytosolic Ca^{2+} overload in Parkinson's disease.
417
418 **Materials and Methods**
419 **Cell lines.** HeLa cervical, human, female carcinoma cells were obtained from the European
420 Collection of Authenticated Cell Cultures (ECACC, 93021013). The TNF-sensitive S1 subclone of
421 human, MCF7 female breast cancer cells has been described previously [61]. MDA-MB-231 (HTB-26)
422 and MDA-MB-468 (HTB-132) human, female breast cancer cell lines, MCF10A (CRL-10317) human
423 female breast epithelial cells, and human kidney HEK-293 (CRL-1573) cells originating from a female
424 fetus were obtained from the American Type Culture Collection (ATCC). TMEM165-KO cell lines
425 were generated using CRISPR/Cas9-mediated gene editing by transfecting single-guide RNA
426 targeting TMEM165 (PXPR001TMEM165) into HeLa and MDA-MB-468 cells, and after 2 weeks
427 clones were picked up and validated by immunoblotting and sequencing. HeLa cells were cultured
428 in Dulbecco's modified Eagle medium (DMEM; Thermo Fisher Scientific, 31966021) supplemented
429 with 10% heat-inactivated fetal calf serum (Thermo Fisher Scientific, 10270-106) and penicillin/
430 streptomycin (Gibco, 15140122). MDA-MB-231 and MDA-MB-468 cells were cultured in DMEM
431 supplemented with 2mM Glutamine, 1x MEM nonessential amino acids solution (Thermo Fisher
432 Scientific, 11140035), 10% heat-inactivated fetal calf serum and penicillin/ streptomycin. MCF-7
433 cells were cultured in RPMI 1640 (Thermo Fisher Scientific, 61870010) supplemented with 10%
434 heat-inactivated fetal calf serum and penicillin/ streptomycin. MCF-10A cells were cultured in
435 DMEM/ F12 (Thermo Fisher Scientific, 31330038) supplemented with 5% horse serum (Thermo
436 Fisher Scientific, 16050-122), 20 ng/ ml epidermal growth factor (Sigma-Aldrich, e-4127), 0.5 µg/ ml
437 hydrocortisone (Sigma-Aldrich, 3867), 100 ng/ ml choleratoxin (Sigma-Aldrich, c-8052), 10 µg/ ml
438 insulin (Sigma-Aldrich, I9278) and penicillin/ streptomycin. HEK293 cells were cultured in DMEM
439 supplemented with penicillin/ streptomycin and 10% fetal bovine serum. All cells were cultured at
440 37°C in a humidified chamber with 95% air and 5% CO_2 and tested regularly for mycoplasma.

441 **Plasmids**. The Lyso-mKeima expression construct was generated by replacing Lyso-GFP in pLV-Lyso-
442 GFP-puro (kindly provided by Dr. Shawn M. Ferguson, Yale University, New Haven, CT) with the first
443 39 amino acids of LAMTOR1 and the GGSGGS linker (Lyso) using restriction sites EcoRI and BamHI.
444 Then the mKeima was inserted into pLV-Lyso-puro using the restriction sites BamHI and XbaI. The
445 TMEM165-mCherry expression construct was generated by inserting mCherry into pLentiCMVie-
446 IRES-BlastR (Addgene #119863) using the restriction sites XhoI and BamHI. Then, the TMEM165
447 cDNA was amplified from pCDNA3.1NEGFP-TMEM165 (Genscript) and inserted into pLentiCMVie-
448 mCherry-BlastR via NheI and XhoI sites. The Lyso-GCaMP8s expression construct was generated by
449 inserting Lyso into pLentiCMVie-IRES-BlastR (Addgene #119863) via the EcoRI and EcoRV sites.
450 Then, the GCaMP8s was amplified from pGP-CMV-jGCaMP8s (Addgene #162371) and inserted into
451 pLentiCMVie-lyso-BlastR using the restriction sites EcoRV and BamHI. The TMEM165-flag
452 expression construct was generated by inserting TMEM165-flag into pLentiCMVie-IRES-BlastR via
453 the NheI and XhoI sites. The TRPML1-GCamP6s expression construct was created by subcloning the
454 human TRPML1 insert from the human TRPML1-EYFP plasmid [62] into the pGP backbone harboring
455 GCaMP6s (Addgene #40753) using restriction sites BglII (N-terminal) and SalI (C-terminal).
456 PXPR001TMEM165 was generated by using the gRNA: GCAGC CGGGG CGCCG AUGCG. Golgi-EGFP
457 (#79809), EGFP-RAB6A (#49469) and LAMP1-mGFP (#34831) were purchased from Addgene.
458 pcDNA3.1+-mCherry was kindly provided by Dr. Christian Wahl-Schott (Biomedical Center, LMU,
459 Munich, Germany).

460 Table 1. Cloning primers

ATG7 sgRNA1S	CACCG CTTTCTCACCAGGTTTTGCA
ATG7 sgRNA1AS	AAAC TGCAAAACCTGGTGAGAAAG C
ATG7 sgRNA2S	CACCG GCTGCCAGCTCGCTTAACAT
ATG7 sgRNA2AS	AAAC ATGTTAAGCGAGCTGGCAGC C
hTRPML1 KozakBglII	ATagatctCGCCGCCACCATGACAGCCCCGGCGG
hTRPML1 GSGSalI	ATgtcgacGCCAGAGCCATTCACCAGCAGCGAATGCTC
GCamP8s NSRV	gc GATATC CGCAAGAAGACCTTCAAGGAG
GCaMP8s CASBamHI	gc GGATCC TTACTTCGCTGTCATCATTTG
Lyso NSkozakEcoRI	gc GAATTC GCCACC ATGGGGTGCTGCTACAGCAG
Lyso ASBamHI	gc GGATCC ACCAGAACCACCGTTGGGC
Lyso ASEcoRV	gc GATATC ACCAGAACCACCGTTGGGC
mCherry CASBamHI	gc GGATCC tca CTTGTACAGCTCGTCCATGC
mCherry NSXhoI	gc CTCGAG ATGGTGAGCAAGGGCGAGGAG
mKeima NSBamHI	gc GGATCC atggtgagcgtgatcgccaag

mKeima CASXbaI	gc TCTAGA TTAGCCCAGCAGGGAGTGGCGG
TMEM165 NSKozakNheI	gc GCTAGC gccacc ATGGCGGCCGCGGCTCCAGG
TMEM165 CASXhoI	gc CTCGAG AAAACCAGAATCAGGGCTTAT
TMEM165flag CASXhoI	gc CTCGAG tca cttatcgtcgtcatccttgtaatc AAAACCAGAATCAGGGCTTAT
TMEM165 sgRNAS	CACCG GCAGC CGGGG CGCCG ATGCG
TMEM165 sgRNAAS	AAAC CGCATCGGCGCCCCGGCTGC C

siRNAs. P2X4: CAAGUCGUGCAUUUAUGAUtt/AUCAUAAAUGCACGACUUGtt, GUCCUCUACUGCAUGAAGAtt/UCUUCAUGCAGUAGAGGACtt. TMEM165: GUAUCUGAAUUG GGUGAUAtt/UAUCACCCAAUUCAGAUACaa,CAGGGUCUAUACAUACUAUtt/AUAGUAUGUAUAGACCC UGaa. TMEM175: GCCUUACACGUUUUCGUUAtt/ UAACGAAAACGUGUAAGGCag, CUGCA UGAUG ACCAU CACC aa/GGTG AUGGT CAUCA UGCAGag.

Antibodies. Anti-α-Tubulin (ab40742), anti-β-Actin (ab20272), anti-GFP (Ab290), anti-Lamin B1 (ab194109), anti-Galectin 1 (ab25138), anti-P4HB (ab137110), anti-EEA1 (ab2900), anti-sodium potassium ATPase (ab76020), and anti-M6PR (ab124767) were purchased from Abcam; anti-GAPDH (5174S), anti-RCAS1 (12290), and anti-VDAC (12454S) from Cell Signaling Technology; anti-LAMP2 (L0668-200UL) from Sigma Aldrich; anti-LAMP1 (sc20011) and anti-Tom20 (sc-11415) from Santa Cruz; anti-TMEM175 (PA5-100355), anti-mouse IgG Alexa Fluor 488 (A-11001), anti-rabbit IgG Alexa Fluor 594 (A-21207), and anti-rabbit IgG Alexa Fluor 488 (A-21206) from Thermo Fisher Scientific; anti-TMEM165 (20485-1-AP) from Proteintech Europe; anti-P2RX4 (APR-002) from Labome; and goat anti-rabbit IgG (PI-1000) from Vector Laboratories.

Chemicals and reagents. Ammonium hydroxide solution (28.0-30.0%) (221228), D-(+)-glucose (G7021), Hoechst-33342 (B2261), iron (II) chloride (372870), iron (III) chloride (157740), NMDG (66930), propidium iodide (P4864), terfenadine (T9652), and valinomycin (V0627) were purchased from Sigma Aldrich. BAPTA-AM (B1205), CellMask™ Green (C37608), ER-Tracker™ Green (E34251), Fluo-4-AM (F14201), HEPES (BP310), LysoTracker™ Deep Red (L12492), LysoTracker™ Green DND-26 (L7526), MitoTracker™ Green (M7514), Nigericin (N1495), and SYTOX™ Green, Nucleic Acid Stain (S7020) were obtained from Thermo Fisher Scientific. ML-SA1 (4746) and thapsigarin (1138) were from Tocris, ebastine (15372) from Caymann, arachidonic acid (HY-109590) from MedchemExpress, concanamycin A (sc-202111) from Santa Cruz, dextran 40 BioChemica (A2249) from PanReac AppliChem, hydrochloric acid (VWRC30024.290) from VWR, MES (02195309-CF) from MP Biomedicals, and EGTA (324626) from Merck.

487 **Transfections.** Plasmid transfections were performed by using TurboFectin 8.0 (Origene, TF81001),
488 Lipofectamine 3000 transfection agent (Thermo Fisher Scientific, L3000008) or Turbofect™
489 (Thermo Fisher, R0531) according to the manufacturer's instructions. siRNA transfections were
490 performed by using Lipofectamine RNAiMax (Thermo Fisher Scientific, 13778075) according to the
491 manufacturer's instructions.
492 **Western blot.** Cell lysates were prepared in Laemmli sample buffer (125 mM Tris, pH 6.7; 20%
493 glycerol; 140mM SDS) supplemented with complete protease inhibitor cocktail (Roche,
494 04693159001) and PhosSTOP™ (Roche, 04906837001), and 0.05 M dithiothreitol and then loaded
495 onto a 4%–20% gradient SDS-polyacrylamide gel for electrophoresis. Proteins were transferred
496 onto polyvinylidene difluoride membranes by using a Bio-Rad Trans-Blot Turbo system. The
497 membranes were blocked with PBS containing 5% milk and 0.1% Tween-20 and incubated with the
498 indicated primary antibodies and corresponding peroxidase-conjugated secondary antibodies. The
499 signal was detected with Clarity Western ECL Substrate and Luminescent Image Reader, and
500 quantified by densitometry with Image Studio Lite software.
501 **Immunostaining.** Cells were grown on coverslips and fixed in 4% paraformaldehyde in Dulbecco
502 phosphate-buffered saline (DPBS; Thermo Fisher Scientific, 14190094) for 20 min were
503 permeabilized with 0.1% saponin in DPBS for 10 min and blocked in 5% goat serum in DPBS for 10
504 min. Sequential incubation of the cells with the indicated primary antibodies and corresponding
505 Alexa Fluor 488- or Alexa Fluor 594-coupled secondary antibodies was performed to label the
506 protein of interest. Nuclei were labeled either with 5 mg/ml Hoechst-33342 or DAPI in the Prolong
507 Gold Antifade Mounting medium. Unless otherwise indicated, images were acquired with an
508 LSM700 microscope with a Plan-Apochromat 63×/1.40 Oil DIC M27 objective and Zen 2010
509 software (all equipment and software from Carl Zeiss, Jena, Germany) and analyzed with Image J
510 (Fiji) software.
511 For live imaging, cells were treated for 10 min with CellMask™ Green dye (1:1000) at 37°C, then
512 treated with LysoTracker™ DeepRed for 30 min at 37°C, washed three times in PBS, treated with a
513 Hoechst-33342 and then processed for live imaging with an Opera Phenix High Content Confocal
514 Imaging System (Revvity).
515 **Ca^{2+} imaging**. For imaging with Fluo-4-AM, ells were stained with 3 mM Fluo-4-AM for 25 minutes in
516 DMEM (Thermo Fisher, 10567014). After two washes with DPBS, the cells were resuspended in
517 Dulbecco's PBS (Gibco, 14190-094) plus 20 mM HEPES. Further incubation with the indicated
518 treatments was performed at 37°C. Relative quantification and comparison of Fluo-4-AM
519 fluorescence were performed using a BD FACSVerse flow cytometer.

520 To measure the absolute $[Ca^{2+}]_{cyt}$, cells were grown in 96-well plates and stained with 3 mM
521 Fluo-4-AM in medium for 25 min. After the indicated treatments, we changed the medium to HBSS
522 (Thermo Fisher Scientific, 14025050) and imaged the cells on the ImageXpress Pico platform. The
523 absolute $[Ca^{2+}]_{cyt}$ was calculated according to

524 $$[Ca^{2+}]_{cyt}=K_d\{(F-F_{min})/(F_{max}-F) \quad (1)$$

525 F is the desired fluorescence intensity measured by the ImageXpress Pico platform; F_{max} is the
526 fluorescence intensity at saturating free Ca^{2+} concentration ($[Ca^{2+}]_{free}$); F_{min} is the fluorescence
527 intensity at zero $[Ca^{2+}]_{free}$; To determine K_d, we stained the cells with 3 mM Fluo-4-AM and then
528 incubated the cells with a series of Ca^{2+} calibration buffers ($[Ca^{2+}]_{free}$ =0, 0.0717, 0.1613, and 39.8
529 µM) supplemented with 10 µM valinomycin, 10 µM nigericin and 3 µM ionomycin for 5 min.
530 Thereafter, the images of the cells were taken with the ImageXpress Pico platform. The obtained
531 fluorescence intensities of Fluo4-AM were used to plot log $\{(F-F_{min})/(F_{max}-F)\}$ vs. Log $[Ca^{2+}]$. The X-
532 intercept from the linear plot is the Log K_d. For the preparation of calcium calibration buffer, the
533 $[Ca^{2+}]_{free}$ was estimated using the equation:

534 $$[Ca^{2+}]_{free}=K_d^{EGTA} \times [CaEGTA/K_2EGTA] \quad (2)$$

535 where K_d^{EGTA} is the dissociation constant of CaEGTA at a given temperature, ionic strength and pH
536 and $[CaEGTA/K_2EGTA]$ is the molar ratio of CaEGTA to K_2EGTA in the particular solution. The table
537 listing K_d^{EGTA} values for CaEGTA in 0.1 M KCl at 37°C can be found through the link
538 (https://biotium.com/wp-content/uploads/2013/07/PI-59100.pdf).

539 HEK293 cells were seeded on 25 mm^2 glass coverslips in standard tissue culture plates (6-
540 well plate, 2 mL of total volume per well) at a density of $2x10^5$ cells per well, i.e., 100,000 cells
541 per mL. After 48 h in culture, the cells were transfected. HEK293 cells were transfected with 1.5 µg
542 of TRPML1-GCaMP6s- or 1 µg of the respective control plasmid or TMEM165-mCherry-carrying
543 plasmid, 4 µL of Turbofect™, and 200 µl of serum-free DMEM per well in a 6-well plate. The cells
544 were then incubated at 37°C for 24 h. Ca^{2+} imaging was performed using an inverted Leica DMi8
545 live cell microscope. First, transfected cells were washed with DMEM and Ca^{2+}-free buffer was used
546 to carefully rinse the wells before placing the glass coverslips into the imaging chamber. All
547 GCaMP6s experiments were conducted in Ca^{2+}-free buffer comprising 138 mM NaCl, 6 mM KCl, 1
548 mM $MgCl_2$, 10 mM HEPES, 5.5 mM D-glucose monohydrate and 2 mM EGTA (adjusted to pH = 7.4
549 with NaOH). Then, 450 µl Ca^{2+}-free buffer was slowly added to the chamber to prevent the cells
550 being washed away. The osmolarity of the Ca^{2+}-free buffer was adjusted to 300 mOsmol/L.
551 GCaMP6s was excited at 470 nm (GFP excitation wavelength) and the emitted fluorescence was
552 captured with a 515 nm longpass filter. mCherry was excited at 568 nm and the emitted
553 fluorescence was captured with a 590 nm filter. Images were obtained every 2.671 sec with a 63x

554 objective. Regions of interest were drawn around each cell coexpressing the GCaMP6s and
555 mCherry constructs. Background areas without cells were selected for manual background
556 subtraction. The fluorescence intensity was calculated using LAS X 5.1.0 software. Baseline values
557 were acquired by averaging fluorescence intensity values from a 30 s recording before the addition
558 of 10 µM ML-SA1. The area under the curve was calculated using GraphPad Prism 9.0.1 software.
559 The mean values per experiment containing 4-12 cells were calculated and used for plotting.
560 **Perilysosomal pH measurement.** Lyso-mKeima expressing cells were grown in 96-well plate and
561 then treated as indicated. Finally, we changed the medium to Live Cell Imaging Solution (Thermo
562 Fisher Scientific, A14291DJ) and obtained images of the cells with the ImageXpress high-content
563 platform. Standard curves used to estimate perilysosomal pH were created by a similar analysis of
564 cells incubated with a series of pH calibration buffers (pH 6.0, 6.5, 7.0, and 7.5; 140 mM NaCl; 2.5
565 mM KCl; 1.8 mM $CaCl_2$; 1mM $MgCl_2$; and 20 mM HEPES) supplemented with 10 µM valinomycin and
566 10 µM nigericin for 5 min.
567 **Lysosomal pH measurement.** To calculate the absolute lysosomal pH, we plated cells in 96-well
568 plates. The next day, the cells were stained with 1 µM LysoSensor Yellow /Blue DND-160 (Thermo
569 Fisher Scientific, L-7545) for 5 minutes, washed twice with DPBS. Then we changed the medium to
570 phenol-red-free DMEM supplemented with high glucose and HEPES (Thermo Fisher Scientific,
571 21063029) and measured the fluorescence of the cells in the SpectraMax iD3 at Ex 329 nm/ Em 440
572 nm and Ex 380 nm/ Em 540 nm. Standard curves used to estimate lysosomal pH were created by a
573 similar analysis of cells incubated with a series of pH calibration buffers (pH 4, 4.5, 5, and 5.5, 15
574 mM HEPES, 130 mM KCl, 1 mM $MgCl_2$) supplemented with 10 µM valinomycin and 10 µM nigericin
575 for 5 min.
576 **Cytosolic pH measurement.** Stably transfected HeLa SypHer3S cells were grown on 96-well plates.
577 After the indicated treatments, the medium was changes to Live Cell Imaging Solution and images
578 were taken with the ImageXpress high-content platform. Standard curves used to estimate
579 cytosolic pH were created by a similar analysis of cells incubated with a series of pH calibration
580 buffers (pH 6, 6.5, 7, and 7.5) supplemented with 10 µM valinomycin and 10 µM nigericin for 5 min.
581 Alternatively, the cells were incubated for 30 min at 37°C in the medium containing an 1:1.000
582 dilution of pHrodo™ Green AM Intracellular pH Indicator (Thermo Fisher Scientific, P-35373) and an
583 1:100 dilution of PowerLoad™ concentrate. The cells were subsequwently washed with Live Cell
584 Imaging Solution and analyzed on an ImageXpress high-content platform.
585 **Whole-cell electrophysiology**. HEK293 cells were seeded on 12 mm^2 glass coverslips in standard 24-
586 well tissue culture plates and were allowed to grow for 24-48 h before transfection. Transfection
587 involved the use of 0.6 µg of total DNA, 2 µL of Turbofect™, and 100 µL of serum-free DMEM per

588 well. Manual patch-clamp recordings of transiently transfected HEK293 cells were carried out in
589 whole-cell configuration. The extracellular/bath solution contained 140 mM NMDG, 10 mM HEPES,
590 10 mM MES, 5 mM EGTA, 5 mM glucose, and 10 nM free [Ca^{2+}] $CaCl_2$ with or without 1 mM $MgCl_2$.
591 The solution was adjusted to either pH 4.6 or 7.5 with MSA. The intracellular/pipette solution
592 contained 140 mM NMDG, 10 mM HEPES, 5 mM EGTA with or without 1 mM $MgCl_2$, and variable
593 concentrations of $CaCl_2$ to reach either 10 nM or 1 µM free [Ca^{2+}]. The pH was adjusted to 7.5 with
594 MSA. The total calcium concentration at each pH was calculated to maintain the indicated amount
595 of free calcium using https://somapp.ucdmc.ucdavis.edu/ pharmacology/
596 bers/maxchelator/CaMgATPEGTA-TS.htm. Recording glass pipettes, with resistances in the range of
597 5-10 MΩ were pulled and polished. Electrophysiological recordings were performed using an EPC10
598 patch-clamp amplifier (HEKA, Lambrecht, Germany), controlled by PatchMaster software (HEKA
599 Elektronik). The compensation circuit of the EPC-10 amplifier cancelled fast and slow capacitive
600 transients. In all the experiments, a step protocol was used: 400 ms voltage steps from -100 to +60
601 mV in 20 mV increments were applied every 5 s for a total of 13 steps, and the holding potential
602 was 0 mV. Digitized and filtered (40 kHz and low-pass filter frequency of 2.9 kHz) current
603 amplitudes at the end (last 5%) of each step, recording from -100 to +60 mV were extracted and
604 normalized to the cell size. All the experiments were conducted at room temperature (22-23°C) and
605 the data were analyzed with GraphPad Prism 10.0.2.
606 **Cell death.** Cells (5000 cells/well) were plated on 96-well plates, and 24 h later, they were treated
607 as indicated. After th eindicated times, the cells were incubated with 0.2 µg/ml propidium iodide or
608 170 nM SYTOX™ Green Nucleic Acid Stain and 2.5 µg/ml Hoechst-33342 for 10 min at 37°C, and cell
609 death was analyzed using a Celigo Imaging Cytometer (Nexcelom Bioscience) according to the
610 manufacturer's instructions.
611 **Preparation of FeDEX solution.** $FeCl_2$ (0.38 g) and $FeCl_3$ (0.73 g) were dissolved in 2.5 ml H_2O each.
612 After the two obtained solutions were mixed, 2.5 ml of 30% (v/v) NH_4OH and 25 ml of 5% (v/v)
613 NH_4OH were added sequentially while a magnetic stirrer was used to stir the solution for 30 mins.
614 After the iron particles had settled, the supernatant was discarded and the iron particles were
615 washed twice with 25 ml H_2O and resuspended in 20 ml 0.3 M HCl with a magnetic stirrer for 30
616 min. Finally, we added 1 g of Dextran 40, stirred the mor for another 30 min and dialyzed the iron
617 dextran solution with H_2O for 24 hours at 4°C.
618 **FeDEX purification.** Cells grown on 15 cm petri dishes were incubated in 20 ml medium containing
619 100 µl of FeDEX solution. The next day, we changed the medium to normal medium. After 2-3
620 hours of chase, the cells were harvested in PBS and washed three times in SuMa buffer (10 mM
621 HEPES; 0.21 M mannitol; 0.07 M sucrose; pH 7.5). The cells were then resuspended in SuMa4 buffer

622 (SuMa 2, 1 µl Benzonase, protease inhibitor) at a concentration of $30x10^6$ cells/ml and
623 homogenized by a gentleMACS Dissociator machine or syringe with a 25G needle. The resulting
624 samples were pelleted by 2x10 min centrifugation at 1500 g. The supernatant was collected as the
625 light membrane fraction (LMF). To further enrich lysosomes containing iron dextran particle, the
626 LMF were passed through MS columns (Miltenyi Biotec, 130-042-201) and the columns were
627 washed three times (once with SuMa4 and twice with SuMa2 (SuMa, 0.5 mM DTT, 0.5% fatty acid-
628 free BSA in SuMa buffer)). Finally, the lysosomal fractions were eluted with 600 µl of SuMa2 from
629 the columns, which were detached from the magnetic stand.
630 **Statistical analysis.** Unless otherwise indicated, the statistical analyses were performed using
631 GraphPad Prism 9 or GraphPad Prism 10 software. Data are shown as means ± SD unless stated
632 otherwise. The specific statistical tests applied are given in the respective figure legends, where
633 statistical significance is given by *P < 0.05, **P < 0.01, and ***P < 0.001; n.s., not significant.
634

635 **Acknowledgments**
636 We thank Shawn M. Ferguson for providing valuable reagents, and Dianna Skousborg Larsen, Louise
637 Vanderfox and Tiina Naumanen Dietrich for the technical assistance.
638 **Funding:** This work was supported by the Danish National Research Foundation grant DNRF125 to
639 M.J., the Danish Cancer Society grants R269-A15695 and R352-A20587 to M.J., the Novo Nordisk
640 Foundation grant NNF19OC0054296 to M.J, and DFG GR4315/2-2, DFG GR4315/7-1, SFB/TRR152
641 P04, and SFB1328 A21 to C.G.
642

643 **Author contributions:**
644 Conceptualization: BL, MJ
645 Methodology: BL, KM, MJ
646 Investigation: RC, BL, DJ, LK, VK, BW
647 Visualization: RC, BL, DJ, LK, VK, BW, YK, AP
648 Supervision: BL, KM, CG, MJ
649 Writing—original draft: BL, MJ
650 Writing—review & editing: RC, BL, DJ, LK, VK, KM, CG, MJ
651

652 **Competing interests:** The authors declare that they have no competing interests.
653

654 **Data and materials availability:** All the data needed to evaluate the conclusions in the paper are
655 present in the paper and the Supplementary Materials. Cell lines, plasmids and data sets generated
656 during the current study will be available from the corresponding authors upon reasonable request.
657
658

659 **References**

660 1. Berridge, M.J., Bootman, M.D. & Roderick, H.L. Calcium signalling: dynamics, homeostasis
661 and remodelling. *Nat Rev Mol Cell Biol* **4**, 517-529 (2003).
662 2. Li, P., Gu, M. & Xu, H. Lysosomal Ion Channels as Decoders of Cellular Signals. *Trends*
663 *Biochem Sci* **44**, 110-124 (2019).
664 3. White, K.A., Grillo-Hill, B.K. & Barber, D.L. Cancer cell behaviors mediated by dysregulated
665 pH dynamics at a glance. *J Cell Sci* **130**, 663-669 (2017).
666 4. Chen, R., Jäättelä, M. & Liu, B. Lysosome as a Central Hub for Rewiring PH Homeostasis in
667 Tumors. *Cancers (Basel)* **12** (2020).
668 5. Flinck, M., Kramer, S.H. & Pedersen, S.F. Roles of pH in control of cell proliferation. *Acta*
669 *Physiol (Oxf)* **223**, e13068 (2018).
670 6. Orrenius, S., Zhivotovsky, B. & Nicotera, P. Regulation of cell death: the calcium-apoptosis
671 link. *Nat Rev Mol Cell Biol* **4**, 552-565 (2003).
672 7. Lagadic-Gossmann, D., Huc, L. & Lecureur, V. Alterations of intracellular pH homeostasis in
673 apoptosis: origins and roles. *Cell Death Differ* **11**, 953-961 (2004).
674 8. de Duve, C., Pressman, B.C., Gianetto, R., Wattiaux, R. & Appelmans, F. Tissue fractionation
675 studies. 6. Intracellular distribution patterns of enzymes in rat-liver tissue. *Biochem J* **60**,
676 604-617 (1955).
677 9. Xu, H. & Ren, D. Lysosomal physiology. *Annu Rev Physiol* **77**, 57-80 (2015).
678 10. Holland, L.K.K., Nielsen, I.O., Maeda, K. & Jaattela, M. SnapShot: Lysosomal Functions. *Cell*
679 **181**, 748-748 e741 (2020).
680 11. Ballabio, A. & Bonifacino, J.S. Lysosomes as dynamic regulators of cell and organismal
681 homeostasis. *Nat Rev Mol Cell Biol* **21**, 101-118 (2020).
682 12. Ellegaard, A.-M., Bach, P. & Jäättelä, M. Targeting cancer lysosomes with good old cationic
683 amphiphilic drugs. *Rev Physiol Biochem Pharmacol* **185**, 107-152 (2023).
684 13. Stahl-Meyer, J., Stahl-Meyer, K. & Jaattela, M. Control of mitosis, inflammation, and cell
685 motility by limited leakage of lysosomes. *Curr Opin Cell Biol* **71**, 29-37 (2021).
686 14. Sterea, A.M., Almasi, S. & El Hiani, Y. The hidden potential of lysosomal ion channels: A new
687 era of oncogenes. *Cell Calcium* **72**, 91-103 (2018).
688 15. Maxson, M.E. & Grinstein, S. The vacuolar-type H(+)-ATPase at a glance - more than a proton
689 pump. *J Cell Sci* **127**, 4987-4993 (2014).
690 16. Stransky, L., Cotter, K. & Forgac, M. The Function of V-ATPases in Cancer. *Physiol Rev* **96**,
691 1071-1091 (2016).
692 17. Hu, M. *et al.* Parkinson's disease-risk protein TMEM175 is a proton-activated proton channel
693 in lysosomes. *Cell* **185**, 2292-2308 e2220 (2022).
694 18. Zheng, W. *et al.* pH regulates potassium conductance and drives a constitutive proton
695 current in human TMEM175. *Sci Adv* **8**, eabm1568 (2022).
696 19. Dolman, N.J. & Tepikin, A.V. Calcium gradients and the Golgi. *Cell Calcium* **40**, 505-512
697 (2006).
698 20. Lloyd-Evans, E. & Waller-Evans, H. Lysosomal Ca(2+) Homeostasis and Signaling in Health
699 and Disease. *Cold Spring Harb Perspect Biol* **12** (2020).
700 21. Morgan, A.J., Platt, F.M., Lloyd-Evans, E. & Galione, A. Molecular mechanisms of
701 endolysosomal Ca2+ signalling in health and disease. *Biochem J* **439**, 349-374 (2011).
702 22. Pittman, J.K. Vacuolar Ca(2+) uptake. *Cell Calcium* **50**, 139-146 (2011).
703 23. Hwang, S.M. *et al.* Intracellular acidification is associated with changes in free cytosolic
704 calcium and inhibition of action potentials in rat trigeminal ganglion. *J Biol Chem* **286**, 1719-
705 1729 (2011).
706 24. Grant, R.L. & Acosta, D. Interactions of intracellular pH and intracellular calcium in primary
707 cultures of rabbit corneal epithelial cells. *In Vitro Cell Dev Biol Anim* **32**, 38-45 (1996).

25. Tanimura, A., Tojyo, Y. & Matsumoto, Y. The cytosolic acidification in rat parotid cells is associated with an increase in cytosolic Ca2+ concentration. *Jpn J Pharmacol* **61**, 357-360 (1993).
26. Gonzalez, A., Camello, P.J., Pariente, J.A. & Salido, G.M. Free cytosolic calcium levels modify intracellular pH in rat pancreatic acini. *Biochem Biophys Res Commun* **230**, 652-656 (1997).
27. Anand, A. *et al.* Cell Death Induced by Cationic Amphiphilic Drugs Depends on Lysosomal Ca(2+) Release and Cyclic AMP. *Mol Cancer Ther* **18**, 1602-1614 (2019).
28. Demaegd, D. *et al.* Newly characterized Golgi-localized family of proteins is involved in calcium and pH homeostasis in yeast and human cells. *Proc Natl Acad Sci U S A* **110**, 6859-6864 (2013).
29. Amick, J., Tharkeshwar, A.K., Talaia, G. & Ferguson, S.M. PQLC2 recruits the C9orf72 complex to lysosomes in response to cationic amino acid starvation. *J Cell Biol* **219** (2020).
30. Tantama, M., Hung, Y.P. & Yellen, G. Imaging intracellular pH in live cells with a genetically encoded red fluorescent protein sensor. *J Am Chem Soc* **133**, 10034-10037 (2011).
31. Tie, H.C. *et al.* A novel imaging method for quantitative Golgi localization reveals differential intra-Golgi trafficking of secretory cargoes. *Mol Biol Cell* **27**, 848-861 (2016).
32. Ellegaard, A.M. *et al.* Repurposing Cationic Amphiphilic Antihistamines for Cancer Treatment. *EBioMedicine* **9**, 130-139 (2016).
33. Petersen, N.H. *et al.* Transformation-associated changes in sphingolipid metabolism sensitize cells to lysosomal cell death induced by inhibitors of acid sphingomyelinase. *Cancer Cell* **24**, 379-393 (2013).
34. Liu, B. *et al.* Cationic amphiphilic antihistamines inhibit STAT3 via Ca 2+ -dependent lysosomal H+ efflux. *Cell Rep* **42**, 112137 (2023).
35. Wu, Y., Huang, P. & Dong, X.P. Lysosomal Calcium Channels in Autophagy and Cancer. *Cancers (Basel)* **13** (2021).
36. Lytton, J., Westlin, M. & Hanley, M.R. Thapsigargin inhibits the sarcoplasmic or endoplasmic reticulum Ca-ATPase family of calcium pumps. *J Biol Chem* **266**, 17067-17071 (1991).
37. Dixon, C.J. *et al.* Extracellular nucleotides stimulate proliferation in MCF-7 breast cancer cells via P2-purinoceptors. *Br J Cancer* **75**, 34-39 (1997).
38. Shen, D. *et al.* Lipid storage disorders block lysosomal trafficking by inhibiting a TRP channel and lysosomal calcium release. *Nat Commun* **3**, 731 (2012).
39. Foulquier, F. *et al.* TMEM165 deficiency causes a congenital disorder of glycosylation. *Am J Hum Genet* **91**, 15-26 (2012).
40. Potelle, S. *et al.* Glycosylation abnormalities in Gdt1p/TMEM165 deficient cells result from a defect in Golgi manganese homeostasis. *Hum Mol Genet* **25**, 1489-1500 (2016).
41. Morelle, W. *et al.* Galactose Supplementation in Patients With TMEM165-CDG Rescues the Glycosylation Defects. *J Clin Endocrinol Metab* **102**, 1375-1386 (2017).
42. Rosnoblet, C. *et al.* Impact of disease-causing mutations on TMEM165 subcellular localization, a recently identified protein involved in CDG-II. *Hum Mol Genet* **22**, 2914-2928 (2013).
43. Haller, T., Dietl, P., Deetjen, P. & Volkl, H. The lysosomal compartment as intracellular calcium store in MDCK cells: a possible involvement in InsP3-mediated Ca2+ release. *Cell Calcium* **19**, 157-165 (1996).
44. Yuan, Y. *et al.* The lysosomotrope GPN mobilises Ca(2+) from acidic organelles. *J Cell Sci* **134** (2021).
45. Aits, S. *et al.* Sensitive detection of lysosomal membrane permeabilization by lysosomal galectin puncta assay. *Autophagy* **11**, 1408-1424 (2015).
46. Sano, O. *et al.* Vacuolin-1 inhibits autophagy by impairing lysosomal maturation via PIKfyve inhibition. *FEBS Lett* **590**, 1576-1585 (2016).
47. Ruas, M. *et al.* Purified TPC isoforms form NAADP receptors with distinct roles for Ca(2+) signaling and endolysosomal trafficking. *Curr Biol* **20**, 703-709 (2010).

759 48. Cao, Q. *et al.* Calcium release through P2X4 activates calmodulin to promote endolysosomal
760 membrane fusion. *J Cell Biol* **209**, 879-894 (2015).
761 49. Medina, D.L. *et al.* Lysosomal calcium signalling regulates autophagy through calcineurin and
762 TFEB. *Nat Cell Biol* **17**, 288-299 (2015).
763 50. Christensen, K.A., Myers, J.T. & Swanson, J.A. pH-dependent regulation of lysosomal calcium
764 in macrophages. *J Cell Sci* **115**, 599-607 (2002).
765 51. Lopez-Sanjurjo, C.I., Tovey, S.C., Prole, D.L. & Taylor, C.W. Lysosomes shape Ins(1,4,5)P3-
766 evoked Ca2+ signals by selectively sequestering Ca2+ released from the endoplasmic
767 reticulum. *J Cell Sci* **126**, 289-300 (2013).
768 52. Garrity, A.G. *et al.* The endoplasmic reticulum, not the pH gradient, drives calcium refilling of
769 lysosomes. *Elife* **5** (2016).
770 53. Atakpa, P., Thillaiappan, N.B., Mataragka, S., Prole, D.L. & Taylor, C.W. IP(3) Receptors
771 Preferentially Associate with ER-Lysosome Contact Sites and Selectively Deliver Ca(2+) to
772 Lysosomes. *Cell Rep* **25**, 3180-3193 e3187 (2018).
773 54. Chadet, S. *et al.* P2x4 receptor promotes mammary cancer progression by sustaining
774 autophagy and associated mesenchymal transition. *Oncogene* (2022).
775 55. Murali, P. *et al.* Novel role for the Golgi membrane protein TMEM165 in control of migration
776 and invasion for breast carcinoma. *Oncotarget* **11**, 2747-2762 (2020).
777 56. Srivastava, J., Barber, D.L. & Jacobson, M.P. Intracellular pH sensors: design principles and
778 functional significance. *Physiology (Bethesda)* **22**, 30-39 (2007).
779 57. Zhang, C.S. *et al.* Fructose-1,6-bisphosphate and aldolase mediate glucose sensing by AMPK.
780 *Nature* **548**, 112-116 (2017).
781 58. Takahara, T., Amemiya, Y., Sugiyama, R., Maki, M. & Shibata, H. Amino acid-dependent
782 control of mTORC1 signaling: a variety of regulatory modes. *J Biomed Sci* **27**, 87 (2020).
783 59. Lawrence, R.E. & Zoncu, R. The lysosome as a cellular centre for signalling, metabolism and
784 quality control. *Nat Cell Biol* **21**, 133-142 (2019).
785 60. Zaichick, S.V., McGrath, K.M. & Caraveo, G. The role of Ca(2+) signaling in Parkinson's
786 disease. *Dis Model Mech* **10**, 519-535 (2017).
787 61. Jaattela, M., Benedict, M., Tewari, M., Shayman, J.A. & Dixit, V.M. Bcl-x and Bcl-2 inhibit TNF
788 and Fas-induced apoptosis and activation of phospholipase A2 in breast carcinoma cells.
789 *Oncogene* **10**, 2297-2305 (1995).
790 62. Grimm, C. *et al.* Small molecule activators of TRPML3. *Chem Biol* **17**, 135-148 (2010).
791

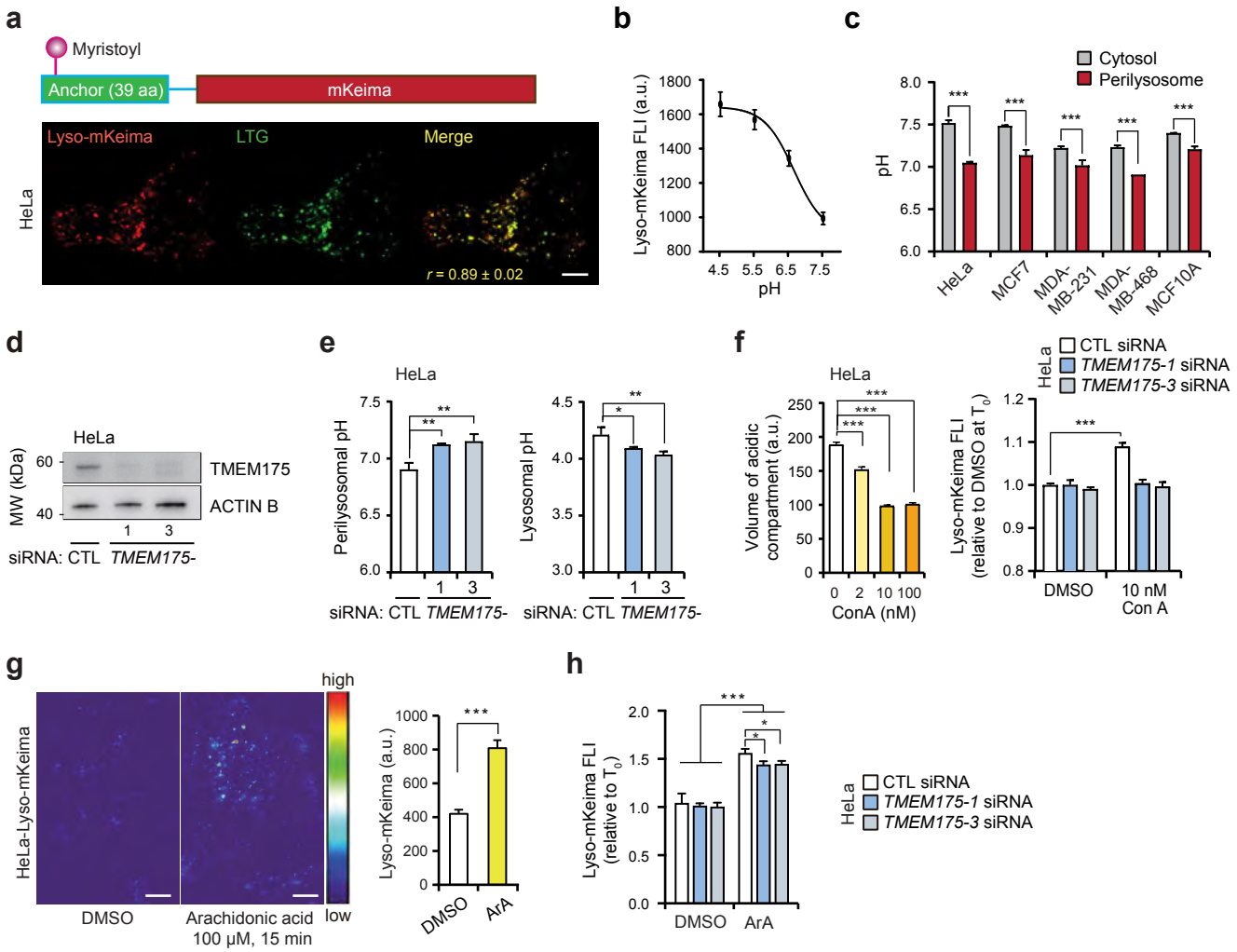

Figure 1. TMEM175 acidifies the perilysosomal area

a. Construct of Lyso-mKeima (top). Representative (n =3) confocal images of live HeLa-Lyso-mKeima stained with Lysotracker® Green (bottom). r, Pearson's colocalization coefficient (n =20). Scale bars, 10 μm.
b. The standard curve for fluorescence intensity (FLI) of mKeima at pH ranging from 4.5 to 7.5.
c. Cytosolic and perilysosomal pH values of indicated cell lines.
d. Representative (n=3) immunoblots of indicated proteins in HeLa cells treated with indicated siRNAs for 72 h.
e. Perilysosomal pH analyzed by Lyso-mKeima (left) and lysosomal pH analyzed by LysoSensorTM Yellow/Blue FLI (right) in HeLa cells treated with indicated siRNAs for 72 h.
f. Relative volumes of acidic compartments in HeLa cells treated with Con A for 1 h, stained with Lysotracker green, and analyzed by flow cytometry (left). mKeima FLI in HeLa-Lyso-mKeima cells treated for 72 h with indicated siRNAs and with either DMSO or 10 nM Con A for 1 h (right).
g. Representative (n = 3) images of live HeLa-Lyso-mKeima cells treated with 100 μM Arachidonic acid for 15 min (left). mKeima FLI of cells shown on left (right).
h. mKeima FLI in HeLa-Lyso-mKeima cells treated for 72 h with indicated siRNAs and with either DMSO or 100 μM Arachidonic acid for 20 min.
Error bars, SD of three independent experiments with ≥10 (a bottom, b, c, e, f right, g, h), or ≥10000 (f left) randomly chosen cells analyzed in each sample. *, $P < 0.05$; **, $P < 0.01$; ***, $P < 0.001$ as analyzed by one-way Anova (e, f left, g right) or two-way Anova (c, f right, h) with Tukey (e, f left, g right) or Dunnett (c, f right, h) multiple comparison.

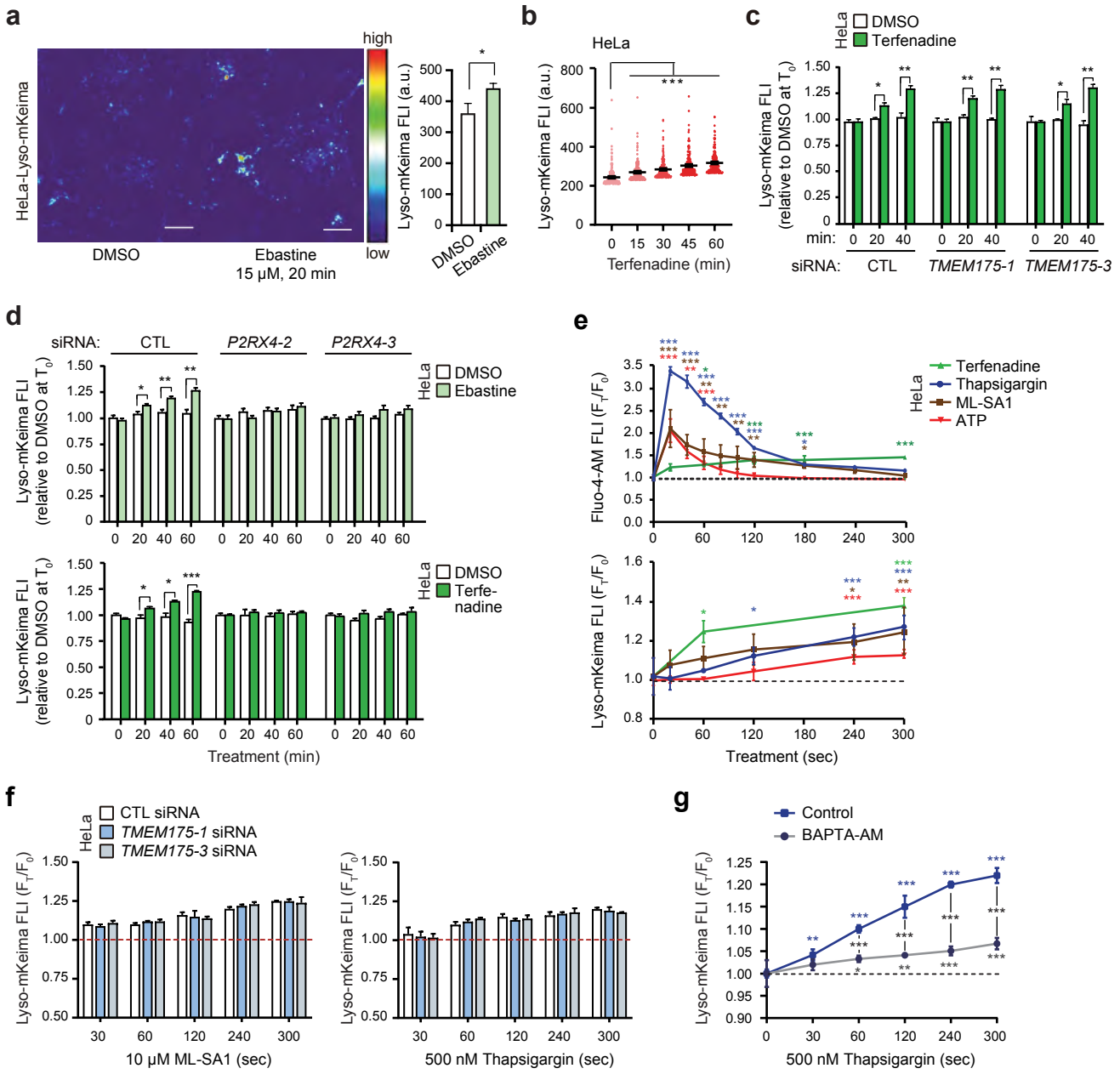

Figure 2. Ca2+ mobilizing agents induce TMEM175-independent lysosomal H+ leak

a. Representative (n = 3) images of live HeLa-Lyso-mKeima cells treated with 15 μM ebastine for 20 min (left). mKeima FLI of cells shown on left (right).
b. Kinetics of mKeima FLI in HeLa cells treated with 6 μM terfenadine.
c. mKeima FLI in HeLa-Lyso-mKeima cells treated for 72 h with indicated siRNAs and with either DMSO or 6 μM terfenadine for the last 20 or 40 min.
d. mKeima FLI in HeLa-Lyso-mKeima cells treated for 72 h with indicated siRNAs and with 15 μM ebastine (top) or 6 μM terfenadine (bottom) for the last 20, 40 or 60 min.
e. Fluo-4-AM FLI (top) and mKeima FLI (bottom) in HeLa cells treated with 6 μM terfenadine, 500 nM thapsigargin, 10 μM ML-SA1 or 1 μM ATP for the last 0 – 300 sec and analyzed by flow cytometry.
f. mKeima FLI in HeLa-Lyso-mKeima cells treated for 72 h with indicated siRNAs and with 10 μM ML-SA1 (left) or 500 nM thapsigargin (right) for the last 0 – 300 sec.
g. mKeima FLI in HeLa-Lyso-mKeima cells pretreated for 30 min with 20 μM BAPTA-AM and treated with 500 nM thapsigargin for the last 0 – 300 sec.
Error bars, SD of three independent experiments with ≥10 (a, b, c, d, f, g), or ≥10000 (e) randomly chosen cells analyzed in each sample. *, P < 0.05; **, P < 0.01; ***, P < 0.001 as analyzed by one-way Anova (a, b) or two-way Anova (c, d, e, f, g) with Tukey (a, b) or Dunnett (c, d, e, f, g) multiple comparison.

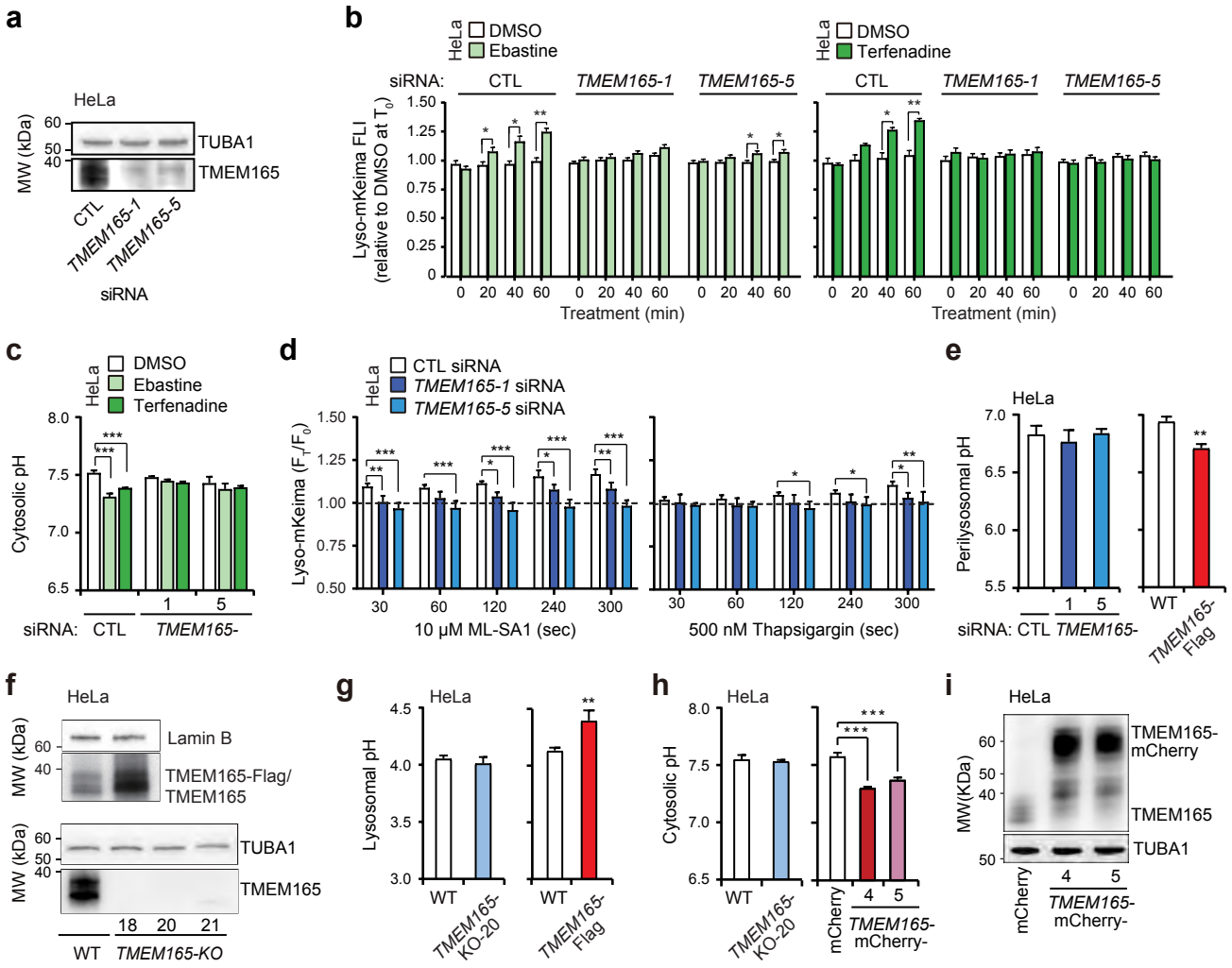

Figure 3. Ca2+-induced lysosomal H+ leak is mediated by TMEM165

a. Representative (n=3) immunoblots of indicated proteins in HeLa cells treated with indicated siRNAs for 72 h.

b. mKeima FLI in HeLa-Lyso-mKeima cells treated for 72 h with indicated siRNAs and with 15 μM ebastine (left) or 6 μM terfenadine (right) for the last 20, 40 or 60 min.

c. Cytosolic pH analyzed by pHrodo-AM FLI in HeLa cells treated with indicated siRNAs for 72 h and with 15 μM ebastine or 6 μM terfenadine for 2 h.

d. mKeima FLI in HeLa-Lyso-mKeima cells treated for 72 h with indicated siRNAs and with 10 μM ML-SA1 (left) or 500 nM thapsigargin (right) for the last 0 – 300 sec.

e. Perilysosomal pH analyzed by Lyso-mKeima FLI in HeLa cells treated with indicated siRNAs for 72 h (left) or in TMEM165 overexpressed cells (right)

f. Representative (n=3) immunoblots of indicated proteins in WT, TMEM165 overexpressed cell lines (top) and TMEM165-KO cell lines (bottom).

g. Lysosomal pH analyzed by LysoSensorTM Yellow/Blue FLI in HeLa TMEM165-KO cells (left) and TMEM165 overexpressed cells (right).

h. Cytosolic pH analyzed by pHrodo-AM FLI in HeLa TMEM165-KO cells (left) and TMEM165 overexpressed cells (right).

i. Representative (n=3) immunoblots of indicated proteins in mCherry- and TMEM165-mCherry-trasfected HeLa clones.

Error bars, SD of three independent experiments with ≥10 randomly chosen cells analyzed in each sample. *, $P < 0.05$; **, $P < 0.01$; ***, $P < 0.001$ as analyzed by one-way Anova (e left, h right) or two-way Anova (b, c, d) with Tukey (e left, h right) or Dunnett (b, c, d) multiple comparison. (e right, g, h left) were analyzed by unpaired t-test.

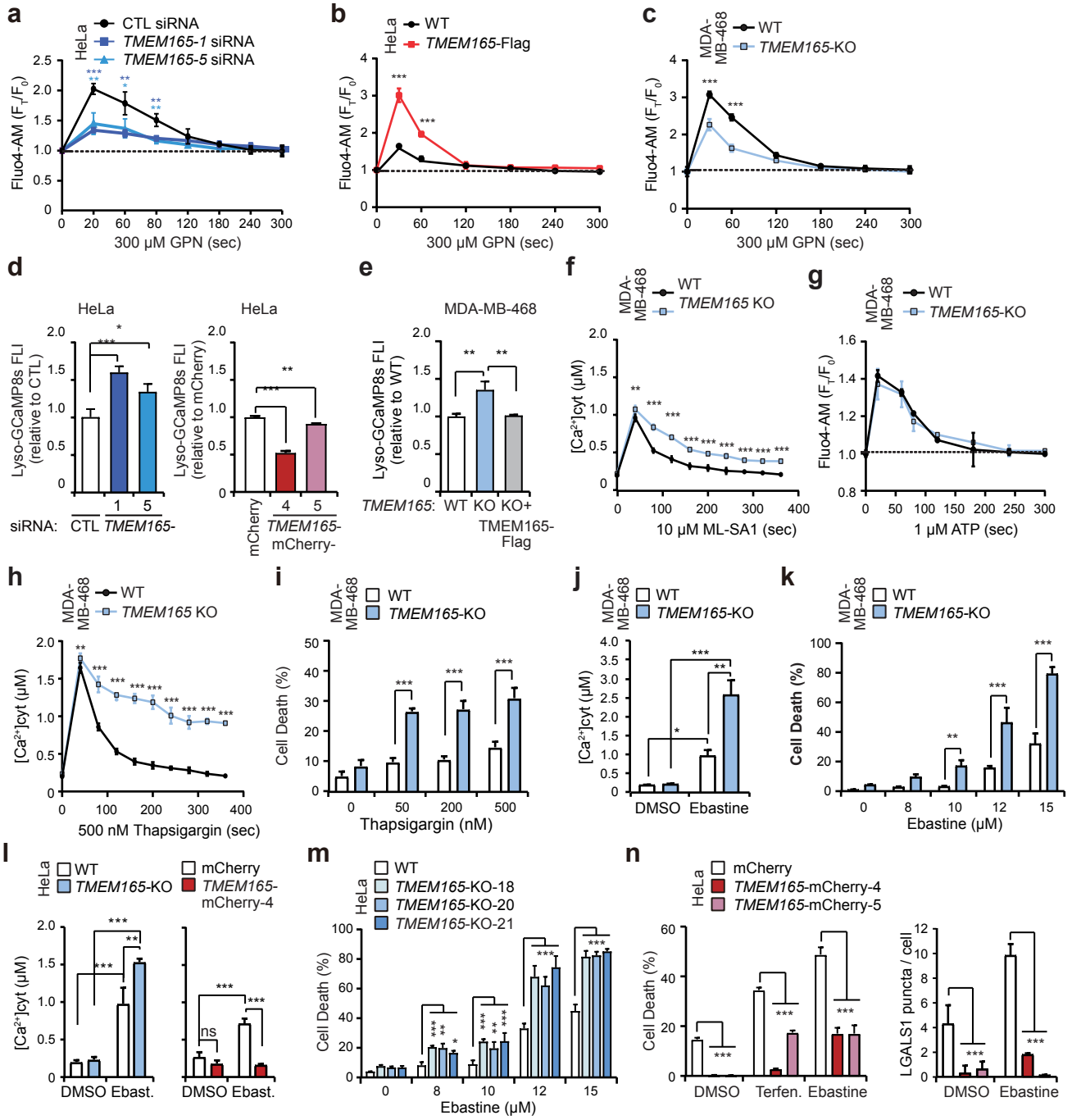

Figure 4. TMEM165 preserves lysosomal Ca2+stores and protects against cytosolic Ca2+ overload

a- c. Fluo-4-AM FLI in HeLa cells treated with indicated siRNAs for 72 h(a), HeLa TMEM165 overexpressed cells (b) and MDA-MB-468 TMEM165-KO cells (c) treated with 300 μM GPN for the last 0 – 300 sec.

d. Lyso-GCaMP8s FLI in Hela cells treated for 72 h with CTL or TMEM165 siRNAs (left) or in HeLa TMEM165 overexpressed cells (right).

e. Lyso-GCaMP8s FLI in indicated cell lines.

f. Cytoslic calcium concentration analyzed by Fluo-4-AM FLI in WT and TMEM165- KO MDA-MB-468 clones treated with 10 μM MLSA1 for the last 0 – 300 sec.

g. Fluo-4-AM FLI in WT and TMEM165- KO MDA-MB-468 clones treated with 1 μM ATP for the last 0 – 300 sec.

h. Cytoslic calcium concentration analyzed by Fluo-4-AM FLI in WT and TMEM165- KO MDA-MB-468 clones treated with 500 nM thapsigargin for the last 0 – 300 sec.

i. Death of indicated MDA-MB-468 cell clones treated with thapsigargin for 24 h. Cells were stained with propidium iodide (dead cells) and Hoechst-33342 (total cells) and cell death was analyzed by Celigo Imaging Cytometer.

j. Cytoslic calcium concentration analyzed by Fluo-4-AM FLI in WT and TMEM165- KO MDA-MB-468 clones with 15 μM ebastine for 1 h.

k. Death of indicated MDA-MB-468 cell clones treated with ebastine for 24 h. Cells were stained with propidium iodide (dead cells) and Hoechst-33342 (total cells) and cell death was analyzed by Celigo Imaging Cytometer.

l. Cytosolic calcium concentration analyzed by Fluo-4-AM FLI in indicated WT and TMEM165- KO HeLa clones (left), mCherry- and TMEM165-mCherry-trasfected HeLa clones (right) with 15 μM ebastine for 1 h.

m. Death of indicated HeLa cell clones treated with ebastine for 24 h. Cells were stained with propidium iodide (dead cells) and Hoechst-33342 (total cells) and cell death was analyzed by Celigo Imaging Cytometer.

n. Death of indicated HeLa cell clones treated with terfenadine or ebastine for 24 h. Cells were stained with SYTOX Green (dead cells) and Hoechst-33342 (total cells) and cell death was analyzed by Celigo Imaging Cytometer (left). Quantification of LGALS1/galectin 1 puncta (leaky lysosomes) in mCherry- and TMEM165-mCherry-trasfected HeLa clones treated with 15 μM ebastine for the last 16 h (right).

Error bars, SD of three independent experiments with ≥10 (f, h, j, l, n right), or ≥10000 (a, b, c, d, e, g, i, k, m, n left) randomly chosen cells analyzed in each sample. *, $P < 0.05$; **, $P < 0.01$; ***, $P < 0.001$ as analyzed by one-way Anova (d, e) or two-way Anova (a, b, c, f, g, h, i, j, k, l, m, n) with Tukey (d, e) or Dunnett (a, b, c, f, g, h, i, j, k, l, m, n) multiple comparison.

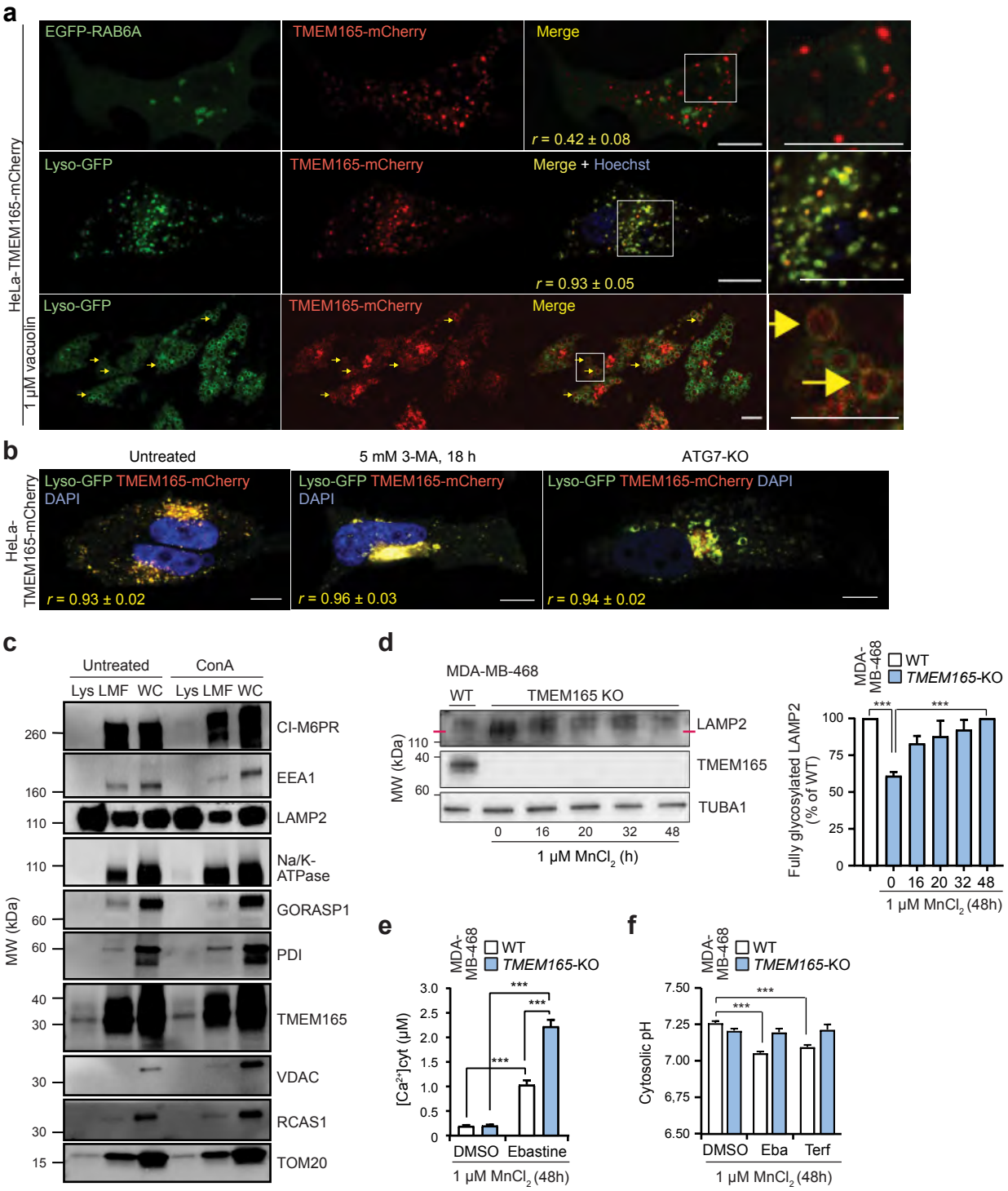

Figure 5. TMEM165 is present on the lysosomal limiting membrane

a. Representative (n = 3) confocal images of live HeLa-TMEM165-mCherry cells transfected with a Golgi marker EGFP-RAB6 (top), or stably expressing Lyso-GFP (middle and bottom). Yellow arrows point to vacuolin-enlarged lysosomes with both Lyso-GFP and TMEM165-mCherry on limiting membranes. DNA is visualized by Hoechst staining. White squares mark the area shown in enlarged images. r, Pearson's co-localization coefficient (n=20). Scale bar, 10 μm.

b. Representative (n=3) confocal images of live HeLa-TMEM165-mCherry-Lyso-EGFP cells with indicated treatments or genetic alteration. r, Pearson's colocalization coefficient (n =20). Scale bars, 10 μm.

c. Representative (n ≥ 3) immunoblots of indicated proteins from purified lysosomes (Lys), light membrane fractions (LMF) and whole cell lysates (WC) of HeLa cells. When indicated, 10 nM concanamycin A (ConA) was added to all buffers used for the extraction.

d. Representative (n = 3) immunoblots of indicated proteins in WT and TMEM165-KO MDA-MB-468 clones treated with 1 μM MnCl2 for indicated times (left), and relative quantification of fully glycosylated LAMP2 (right).

e. Cytoslic Ca2+ concentration analyzed by Fluo-4-AM FLI in WT and TMEM165- KO MDA-MB-468 clones treated with DMSO or 15 μM ebastine for the last 1 h of the 48 h treatment with 1 μM MnCl2.

f. Cytosolic pH analyzed by pHrodo-AM FLI in WT and TMEM165- KO MDA-MB-468 clones treated with DMSO, 6 μM terfenadine, or 15 μM ebastine for the last 1 h of the 48 h treatment with 1 μM MnCl2.

Error bars, SD of three independent experiments with ≥10 randomly chosen cells analyzed in each sample. *, P < 0.05; **, P < 0.01; ***, P < 0.001 as analyzed by by one-way Anova (d right) or two-way Anova (e, f) with Tukey (d right) or Dunnett (e, f) multiple comparison.

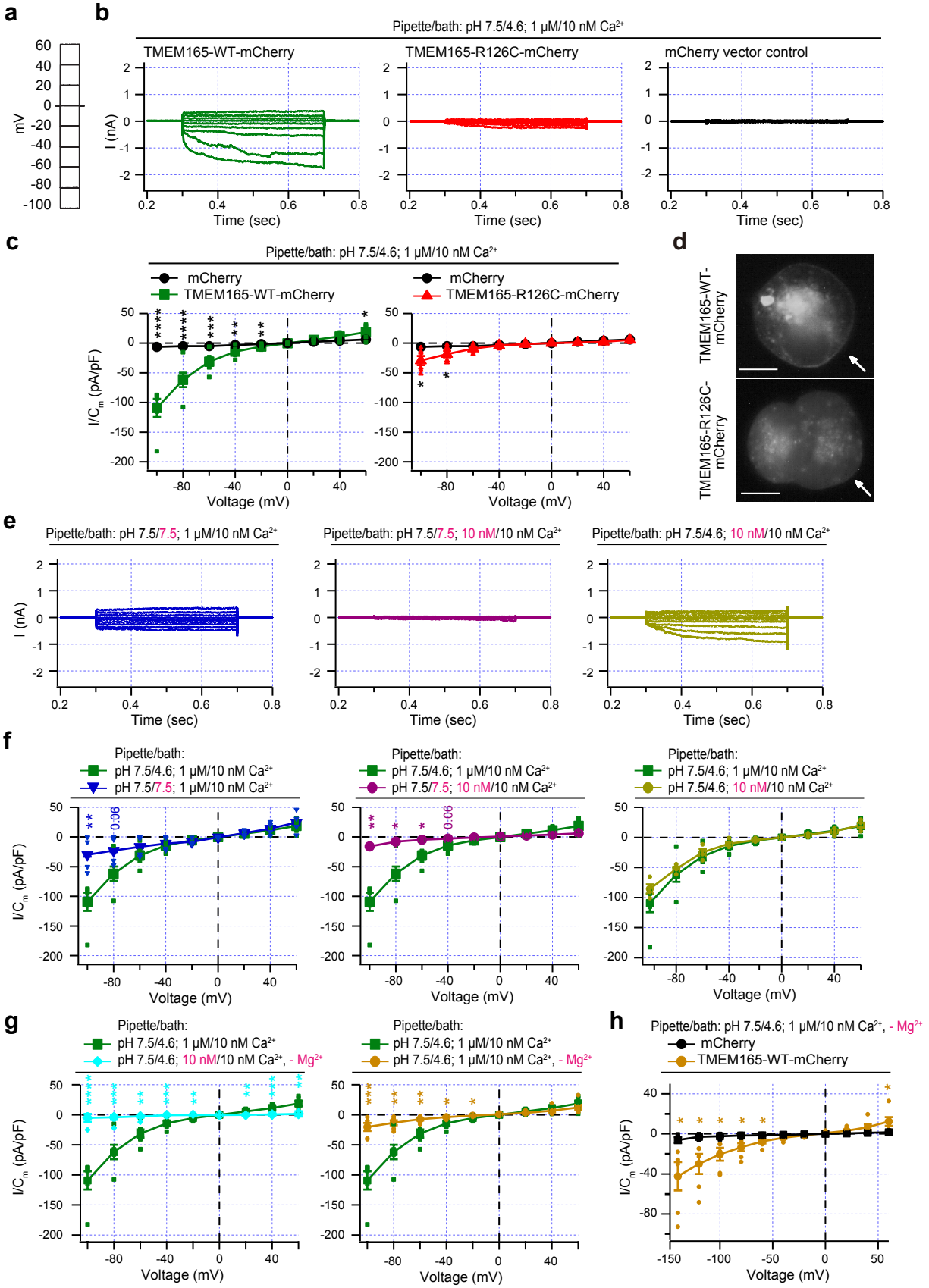

Figure 6. TMEM165 mediates H+ inward and Ca2+ outward currents
a. Voltage step protocol employed for current recordings. **b**. Examples of macroscopic current recordings conducted for TMEM165-WT-mCherry (green), TMEM165-R126C-mCherry mutant (R126C, red), and mCherry control (black) transiently expressed in HEK293 cells. Measurements were performed using indicated pH and Ca2+ concentrations in the pipette/bath. **c**. Current densities plotted against respective voltages for TMEM165-WT-mCherry (left, green squares, n=6) and TMEM165-R126C-mCherry (right, red triangles, n=6) and the control (black circles, n=12). **d**. Representative live images of HEK293 cells transiently transfected with TMEM165-WT-mCherry or TMEM165-R126C-mCherry. Arrows, plasma membrane; scale bars, 10 μm. **e**. Examples of macroscopic current recordings for TMEM165-WT-mCherry using indicated pH and Ca2+ concentrations in the pipette/bath. **f**. Current densities plotted against respective voltages for TMEM165-WT-mCherry at indicated pH and Ca2+ concentrations in the pipette/bath solution with asymmetrical Ca2+ and pH (green squares, n=6) or asymmetrical Ca2+ and symmetrical pH (blue reverted triangles, n=4), symmetrical Ca2+ and symmetrical pH (magenta circles, n=3), and symmetrical Ca2+ and asymmetrical pH (mustard circles, n=4). **g**. Current densities plotted against respective voltages for TMEM165-WT-mCherry at indicated pH and Ca2+ concentrations in the pipette/bath solution with asymmetrical Ca2+ and pH with Mg2+ (green squares, n=6) and without Mg2+ (mustard circles, n=6, right) or symmetrical Ca2+ and asymmetrical pH without Mg2+ (cyan circles n=7, left). **h**. Current densities plotted against respective voltages for TMEM165-WT-mCherry (orange circles, n=6) and mCherry control (black squares n=6) at indicated pH and Ca2+ concentrations in the pipette/bath solution with asymmetrical Ca2+ and pH, and without Mg2+. Error bars, ± SEM; *, P < 0.05; **, P < 0.01; ***, P < 0.001, ****, P < 0.0001, or as analyzed by unpaired t-test using GraphPad Prism 10.0.2.